Revision 1

Microbial and inorganic control on the composition of clay from volcanic glass alteration experiments

Javier Cuadros[1*], Beytullah Afsin[1**], Premroy Jadubansa[2], Mahmoud Ardakani[3], Carmen Ascaso[4] and Jacek Wierzchos[4]

[1]Department of Mineralogy, Natural History Museum, Cromwell Road, London SW7 5BD, UK

[2]Department of Zoology, Natural History Museum, Cromwell Road, London SW7 5BD, UK

[3]Department of Materials, Faculty of Engineering, Imperial College London, London SW7 2AZ, UK

[4]Department of Environmental Biology, National Museum of Natural Sciences, CSIC, Serrano 115, 28006 Madrid, Spain

*Corresponding author: j.cuadros@nhm.ac.uk;

**Present address: Department of Chemistry, Faculty of Science and Arts, Ondokuz Mayis University, Samsun, 55139 Turkey

Short title: Microbial and inorganic control on neoformed clay

Abstract

Biological activity plays a substantial role in the geochemistry of the Earth's surface. Particularly interesting are effects on clay formation because clays are abundant and have high surface-to-volume ratio, resulting in clays making up a large fraction of the overall mineral-fluid interface and having an effective control of mineral reactions. Thus, biological control on clay composition would affect element budget globally and the mineralogy of subsequent diagenetic processes. Biological acceleration of clay production would result in enhanced clay control of mineral reactions and faster organic C sequestration, by adsorption on clay minerals, with implications for the C and related cycles. We investigated the combined effect of microbial activity and water chemistry on the composition of neoformed clay by reacting volcanic glass with natural waters covering a large composition range (fresh water from a lake and a spring, seawater, and hypersaline water). The microbes (bacteria, fungi and algae) were totally or partially identified using molecular and microscopy techniques. The solid alteration products were analyzed using cryo-SEM to investigate the mineral-microbe interface and TEM-AEM to study the composition of the neoformed clay. The solution chemistry was also investigated. We found that clay composition was controlled mainly by glass chemistry, rather than biological activity, through a mechanism of in situ transformation. The resulting clay was Al-rich (dioctahedral composition). In one case (inorganic experiment, freshwater lake), the specific inorganic conditions of pH and Mg and Si concentration promoted formation of Mg-rich (trioctahedral clay). Microbes, however, did influence clay composition by confining glass grains in biofilms where water chemistry is significantly different from the bulk solution. Alteration in such conditions generated significant amounts of trioctahedral, Mg-rich clay in the hypersaline water experiment, whereas it favoured production of dioctahedral, Al-rich clay in the freshwater lake experiment. It is thus demonstrated that biofilms can exert an effective control on clay mineralogy.

Keywords: Cryo-SEM; Glass alteration; Mechanism of clay formation; Microbial control on clay generation; TEM-AEM.

Introduction

Clay formation and transformation represents a significant volume of the geochemical reactions at the Earth's surface (Brownlow, 1996), which in addition of their large surface area, causes them to exert a large control on geochemical reactions in the crust (Cuadros, 2012). Thus, the influence of microbial activity on clay formation and composition, and the relative importance of such effect with respect to inorganic variables (rock and water chemistry, temperature, etc.) are essential information to fully understand the geochemical processes operating near the Earth's surface. Conversely, clays have an important effect on the biota as they provide physical support as well as accessible water and nutrients, organic and inorganic, through cation exchange, colloid and organic adsorption and their own degradation (Chorover et al., 2007). Although the inorganic conditions that control the composition of neoformed clay minerals are roughly understood and physicochemical environments are successfully related to clay mineralogy and chemistry (Chamley, 1989), there are frequent exceptions to such accepted knowledge, seemingly related to the scale and duration of the alteration process. In the early stages of the alteration process, clay mineralogy and chemistry appears to be controlled preferentially by the altered rock, with little or no effect from the chemistry of altering waters (Ghiara et al., 1993; de la Fuente et al., 2002; Proust et al., 2006). The products of thorough alteration, however, indicate much greater input from the water chemistry (Caballero et al., 1992; Christidis, 2008). Clays formed by mediation of biological activity tend to have low crystallinity (Sanchez-Navas et al., 1998; Konhauser and Urrutia, 1999) and variable composition, which suggests a complex combination of controls on clay chemistry among which the mechanism of clay formation is important. Such mechanisms include crystallization in contact with cell walls (Urrutia and Beveridge, 1994; Tazaki, 2005), with extracellular polymeric substances (EPS) secreted by the microorganisms (Barker and Banfield, 1996; Ueshima and Tazaki,

2001) and precipitation within the cation-enriched biofilms (Sanchez-Navas et al., 1998). The present work aims at shedding further light on the inorganic and biological controls on clay formation. Four representative types of water with their microbial fauna (enhanced or suppressed by addition or lack of organic nutrients) were reacted with rhyolitic volcanic glass. The contribution of both water chemistry and biological activity to clay chemistry was evaluated. The questions asked were, do waters of very different chemistry produce clays of different composition? Do microorganisms control the composition of neoformed clay above the inorganic parameters? Do microorganisms accelerate clay formation? Volcanic glass was selected because alteration reactions develop faster than in crystalline phases.

Experimental

Reactions

Rhyolitic volcanic glass with significant Fe and Mg content was chosen to extend the range of available inorganic nutrients. Two glasses (feldspar traces as the only crystalline phase), from Lipari and Milos (collections of the Department of Geology and Paleontology, and Museum of Mineralogy at the Faculty of Geology and Geography, both at the University of Sofia), were mixed (mass ratio of Lipari/Milos=3.34) to obtain the amount necessary for the experiments. They were ground, homogenized and dry-sieved to a 150-250 μm size-range. The mixture was chemically analyzed (Table 1) after acid attack with HF-$HClO_4$-aqua regia attack in closed bottles in a microwave oven (Thompson and Walsh, 2003), using inductively coupled plasma-atomic emission spectrometry (ICP-AES, in a Varian VISTA PRO). Analytical errors were ±0.2-2.5 % (σ) of the measured values. The detection limits ranged from 5 ppm for Sr to 0.05 wt % for CaO.

Four types of natural water were used: spring water (Compton-Abdale, UK), seawater (Brighton, UK), fresh water (West Reservoir, London, UK) and hypersaline water (Las Saladas de Chiprana, Spain). These waters are representative of the major types on Earth's surface. The waters were

collected avoiding sediment, filtered (8 μm pore size) and transferred to the experiments within 48 h. Experiments were performed with and without biological activity. The glass (1 g) and water (250 ml) were placed in sterile bottles. The bottles with the inorganic experiments (no biological activity) were closed and kept in the dark. This procedure does not eliminate biological activity completely but proved to reduce it to unobservable levels (i.e., no visual development; see below that microbial development in biological experiments resulted in large biomats). The waters could not be sterilized by heating without altering their chemistry and UV treatment of the large volume required proved ineffective. The lack of light eliminated development of photosynthetic organisms and the lack of organic nutrient avoided development of heterotrophes. Organic nutrients (1-3 mg of glucose and peptone) were added to the biological experiments every 2 weeks. The cap of the bottles was not tightened to allow gas diffusion. For the first few weeks, the cap was removed daily for a few hours to allow microbial contamination and foster biological activity. The bottles were illuminated 12 h a day with artificial greenhouse white light. For all experiments, the usual temperature range was 20-24ºC (absolute range 18.0-28.8ºC) and the average 22ºC. Experiment duration was 6, 10, 14 (1 replicate) and 18 months (3 replicates). After the experiments, the reacted glass from hypersaline and seawater was washed with deionized water to minimize salt precipitation.

Water analyses

Waters were double filtered (8 μm pore size) and chemically analyzed before and after the experiments for a suit of cations (ICP-AES, using a Varian VISTA PRO) and pH (±0.02 pH units uncertainty). Anions were measured in the original waters only (ion chromatography, Dionex DX300) because the added nutrients in the biological experiments produced a large interference. The complete anion concentrations are not shown; they were used to assess speciation in some solutions. Cation detection limits were 0.002-0.1 mg/L, depending on the cation, and uncertainty ±0.1-10% (σ) of the value, depending on element concentration. Anion detection limits in the spring and freshwater lake were 0.02-0.17 mg/L, depending on the anion, and for sea and hypersaline

water 1-8.5 mg/L. Uncertainty was ±3% (σ) of the value for fluoride and ±1% (σ) for other anions. Silicon concentration was below 5 mg/L in all original waters (Fig. 1). The spring water was dominated by Ca (104 mg/L) and CO_3^{2-} (132 mg/L), with lower levels of Na, Mg, K (5-0.8 mg/L; Fig. 1), NO_3^- (51.9 mg/L), SO_4^{2-} (21.2 mg/L), and Cl^- (11.3 mg/L). The fresh water from the lake was dominated by Ca (44.0 mg/L), Na (33.2 mg/L), CO_3^{2-} (60 mg/L), Cl^- (50.1 mg/L), and SO_4^{2-} (44.1 mg/L), with lower Mg and K (6.4-4.6 mg/L). The composition of the seawater was entirely typical, dominated by Na (10.4 g/L), Mg (1.2 g/L), Cl^- (19.6 g/L), and SO_4^{2-} (2.7 g/L). The major components of the hypersaline water were Na (18.9 g/L), Mg (16.0 g/L), SO_4^{2-} (84.5 g/L), and Cl^- (26.2 g/L). The pH values of the original solutions were within 7.5-8.2, except the fresh water from the lake, with a value of 9.0.

Analysis of microbial species

Microbial species (bacteria, fungi and algae) in the original waters, glass, air in the room where the experiments were conducted and in the waters after the experiments (6 and 14 months, in the biological tests only) were identified or some approach to identification was conducted.

A sample of the volcanic glass was placed in 30 mL of sterilized water, stirred vigorously for 10 minutes and the water was then used in the procedure indicated below. Specific media were prepared for bacteria (nutrient agar from Oxoid), fungi (malt extract agar from Oxoid and Streptomycin and Chlorotetracyclene antibiotics from Sigma Aldrich) and algae and cyanobacteria (3N-BBM+V medium for freshwater algae, F/2 for marine algae, both from Culture Collection for Algae and Protozoa, and BG-11 from Sigma Aldrich for cyanobacteria). One hundred microlitres of the water (original waters or water from the procedure to extract biota from the volcanic glass) were pipetted on the corresponding medium with a sterilized pipette. For sampling of the air in the laboratory, two media of each type were left open in the room, for 2 h in the case of bacterial media plates, 2 days for fungi and 6 weeks for algal media plates. After sampling, the bacterium media

were kept at room temperature for 2 days and fungus media were incubated at 25 ºC for 1-2 weeks. The algal media were kept for 4-6 months. Bacterial and fungal species were isolated by repeated subculturing on the same media and finally stored at 4 ºC.

Algae were visually examined to provide an approximate identification or a description of their morphology, using light microscopes. Bacteria were studied by Gram staining and examination with a light microscope to obtain their staining characteristics and morphology. Bacteria and fungi were further identified using molecular analysis. The DNA was extracted using Power Soil DNA Isolation Kit from Cambio. The 16S (bacteria) and 18S (fungi) rDNA region containing information about the species identity was amplified using Polymerase Chain Reaction (PCR) with a Perkin Elmer GeneAmp PCR System 9600. Amplitaq Gold PCR mix from Applied Biosystems, and pE* and pA primers from Sigma Aldrich were used. The amplified fragments were sequenced with a 3730xl DNA Analyzer from Applied Biosystems and the species identified by matching the sequences against a database of DNA sequences using BLAST (Basic Local Alignment Search Tool). The visual inspection of algae and the molecular analysis of bacteria and fungi were carried out also in the experiments after 6 and 14 months to acquire information about the dynamics of the microbial population.

Cryo-SEM analysis

Biological 18-month experiments (one replica of each) were analysed with cryo-SEM to investigate the relation between biofilms, glass, and neoformed minerals. Pieces of the biofilm containing glass grains were sampled and placed in water-saturated atmosphere until analysis. Immediately previous to analysis, they were frozen in subcooled liquid N_2 (-170 ºC), fractured to allow observation of mineral-biofilm contact, etched at -70 ºC for ~ 5 minutes (ice sublimation to allow observation of the sample surface), and Au-coated. Operations after freezing were carried out in an Oxford Cryotrans CT-1500 unit, attached to the microscope, which is a Zeiss 960 SEM apparatus. Samples

were viewed using both back-scattered and secondary electrons, and chemically analyzed using an Oxford Link Isis EDX detector.

TEM-AEM analysis

One of each 18-month samples, biological experiments and controls, were analyzed using TEM-AEM to characterize the type of clay products. Some glass grains and part of the biological mat (from biological experiments) were transferred to wide plastic vials. The dry biological mat was broken in fragments. Ethanol of reagent grade was added and the suspension sonified (ultrasound probe) at 60 watts for 30 s. The suspensions were shaken, let to settle for a few minutes, and a few drops from the upper part of the suspension were sampled and deposited on a Cu microgrid with a Formvar film stabilized with C. The study was carried out in a Jeol 2010 TEM apparatus at 200 kV. Chemical analysis (AEM) was performed using an X-Max 80 mm^2 Oxford Instruments detector with Inca software, with acquisition live time of 60 s, after quantitative optimization using the Cu microgrid. The composition of 2:1 phyllosilicate particles was transformed into structural formulas on the basis of $O_{10}(OH)_2$. The criteria followed were the following. All Si and necessary Al were used to complete the 4 tetrahedral positions. The remaining Al and all Fe (assumed to be Fe[III]) and Mg were assigned to the octahedral sheet. Potassium and Na were assigned to the interlayer sites.

Results

There was a large microbial development in the biological experiments. All but the seawater experiments developed a thick biofilm that enveloped the glass grains in a single mass. In the seawater experiments, an extensive, loose biofilm covered the glass grains without holding them together. The microbial colonies contained bacteria, fungi, algae and protozoa (no identification of protozoa was intended), and evolved during the experiments (Table 2). Bacteria developed quickly and, seemingly, many of their species disappeared during the experiments. Most fungi and algae

206 needed a longer time or a developed ecosystem to proliferate. Molecular identification of fungi was
207 difficult and frequently unsuccessful. The control experiments showed no apparent biological
208 development.
209
210 The cation concentrations in the solutions of biological and control experiments at all reaction times
211 were typically similar (Fig. 1). Some variations existed between biological and control experiments
212 (e.g., Fig. 1, Ca in spring water) and between the replicas of the 18-month biological experiments
213 (e.g., Fig. 1, Na in spring water). These variations indicated modifications produced by the
214 biological activity and differences between the specific biological colonies generated in each
215 experiment. The most defined chemical trend was an exponential increase of dissolved Si with time,
216 except for seawater. Other cations displayed decrease-increase concentration cycles. The pH values
217 were slightly higher (up to 0.6 units) in the biological tests. Iron and Al concentrations were
218 typically below the detection limit. For Fe, the detection limit range was 0.01-0.5 mg/L, depending
219 on the dilution due to water salinity. Measured Fe contents were 0.016 mg/L from the original lake
220 fresh water and 6.9-9.3 mg/L in the 18-month experiments with hypersaline water, both biological
221 and inorganic. For Al, the detection limit ranged 0.04-1.0 mg/L. The few Al concentrations
222 measured were in the range 0.041-0.063 mg/L.
223
224 The cryo-SEM study was aimed at investigating the interface between the biofilms and the mineral
225 grains, and thus only carried out on the biological experiments. These analyses showed how the
226 biofilm (network of EPS and microorganisms) encapsulated or coated the glass grains (Fig. 2a-b).
227 Most glass grains revealed pristine surfaces and glass corrosion features were infrequent, although,
228 at times, there were signs of alteration, described below. In the hypersaline water experiments, the
229 inner biofilm medium was a salt brine that crystallized in the cryo-chamber (Fig. 2a). The ion
230 concentrations within the biofilms in the fresh water from the lake and spring were lower and there
231 was no salt crystallization occupying the entire volume between glass grains, as with the

hypersaline water. However, from the hypersaline water and literature results (Sánchez-Navas et al., 1998; Aouad et al., 2006), it is assumed that the fluid within the biofilm in freshwater experiments was more concentrated and had a different composition than the bulk solution.

SEM images revealed a range of glass alteration features that were not distinct for the several types of water. These images showed silicate grains of variable Al-Fe-Mg content, compatible with altered glass or neoformed clay and glass mixtures. They appeared in the biofilm-glass interface, mixed with grains of a Ca-rich phase (most likely carbonates, which were abundant as shown by infra-red analysis; not shown) and on the glass surface (Fig. 2b-c). Analyses focused on the latter because they could be chemically analyzed with the least interference from other phases (however, the quantitative chemical analysis results of alteration products is described with the TEM study below). They had compositions intermediate between clay and glass, which could indicate either thin clay layers on glass or intermediate stages of glass alteration into clay. In addition, some glass grains showed small platy particles that appeared to form in situ (Fig. 2d). The small size of these particles prevented chemical analysis due to the large background glass contribution. These platy particles are interpreted to result from the transformation of the glass surface into clay, whether complete or incomplete. Similar alteration morphology was observed in experimental hydrothermal alteration of volcanic glass and interpreted in the same way (de la Fuente et al., 2000; Fiore et al., 2001). Similarly, particles on the surface of experimentally altered obsidian, although with different morphology, appeared to evolve from allophane to smectite (Kawano et al., 1993).

TEM-AEM analyses revealed a variety of fine particles of compositions indicating salts (mainly chlorides and sulphates), Ca-rich phases of carbonate or organic nature, and silicates. The carbonates are likely calcite, a frequent product of microbial activity (Ehrlich, 1998). Phases detected less frequently were alunite, with a distinctive Al-K-S signature, and oxides and oxihydroxides, as indicated by compositions entirely dominated by Fe, Mg, Al or Ti. We did not

observe grains with compositions consisting with hydrotalcite. This mineral is sometimes found as a transient product during the alteration of volcanic glass in Mg-containing systems (Thomassin et al., 1989; Abdelouas et al., 1994). The silicate particles with compositions consistent with clays also had the typical flaky clay morphology, usually with irregular outlines (Fig. 3). Some clay-like particles showed glass morphology as indicated by very sharp edges and outline (Fig. 3a). Such particles support a glass transformation process for clay formation, as suggested by the SEM results. The alteration of volcanic glass grains into clay with the preservation of the original glass morphology has been observed before in hydrothermal alteration of volcanic glass (de la Fuente et al., 2000), and the mechanism of in situ alteration of glass into clay has been described in synthetic (Thomassin et al., 1989) and natural (Alt and Mata, 2000) basaltic glass, as well as in rhyolitic glass (Fiore et al., 2001). In our results, clay particles with glass-related morphology (Fig. 3a) or comparatively large lateral dimensions (> 2 μm in the largest axis) had beidellite-like and K-rich composition (Figure 3a,c).

AEM analyses of silicate particles (typically < 1 μm) were screened using their atomic ratios to identify those corresponding to clays. It was assumed that smectite would be the most likely clay product. The phyllosilicate nature of a few particles was ascertained using electron diffraction (SAED), which showed either typical hexagonal patterns (Fig. 3b) with variable extent of streaking or weak, undefined patterns. Such behaviour is compatible with smectite, where the small particle size, the few layers in individual crystallites, the relative rotation of the layers, and the curling of the layers with the concomitant lack of uniform crystal orientation all add to produce weak and poor SAED patterns. Indeed, smectite particles with high degree of layer orientation (Fig. 3b) are rather uncommon. Most cases, the clay nature of the particles was based on their chemical composition. The criterion followed for the selection was $1 \leq (Si / Al+Mg+Fe) \leq 2$, which covers the composition range of smectite and other 2:1 phyllosilicates (Si ≈ 3-4 atoms per half formula unit) of dioctahedral (Al+Mg+Fe ≈ 2) and trioctahedral (Mg+Al+Fe ≈ 3) character.

284

285 The plot of Si / (Al+Mg+Fe) vs. Al / Si ratios from particles with Si, Al, Mg, and Fe as the largely
286 major or only components (Fig. 4) shows abundant particles with composition compatible with Al-
287 rich, dioctahedral clay from montmorillonitic to beidellitic (or illitic, see below) character. Fewer
288 particles have a composition compatible with Mg-rich, trioctahedral clay, mainly in the inorganic
289 experiments with lake fresh water and the biological experiments with hypersaline water. Other data
290 points (outside the fields in Fig. 4) probably correspond to altered glass with both, increased and
291 decreased Al-Mg-Fe contents. The plots corresponding to spring, sea and hypersaline water suggest
292 a continuum of chemical changes from the glass that has two opposed trends, one corresponding to
293 Al-Mg-Fe depletion (Si / [Al+Mg+Fe] > 4, Fig. 4; these analyses also display Na, K and Ca
294 depletion) and the other trend corresponding to an increase of Al-Mg-Fe relative to Si, towards the
295 dioctahedral clay fields (Fig. 4). The data points within the trioctahedral field and below it are not
296 part from the above trend and do not show any specific chemical pathway of their own from the
297 circumference marking the composition of the original glass.

298

299 Similar plots using Mg / Si in the x-axis were created (Fig. 5) to test whether some trend would
300 become apparent between the chemical compositions of the glass and the particles within the
301 trioctahedral field. The only trend occurs in the spring water experiments, where the data points are
302 distributed along two lines joining at Mg / Si ~ 0.1. In the other cases, the data are distributed
303 approximately in independent vertical and horizontal arrangements.

304

305 The compositions within the clay fields in Figures 4 and 5 were transformed into structural
306 formulas for 2:1 phyllosilicates (Table 3). The results are good matches with smectite of
307 composition ranging from dioctahedral to trioctahedral. Calcium was not detected in analyses of
308 phyllosilicates. Rather, it frequently appeared with S (in good stoichiometric correspondence with
309 gypsum) or in likely carbonate or oxalate phases. The fact that the octahedral occupancy indicates

the existence of di- and trioctahedral components in many of the analyses may indicate the existence of layers of one and the other composition or the existence of di- and trioctahedral domains within layers (Deocampo et al., 2009). Although smectite is the expected clay product at low temperature, there are frequent cases in which the layer charge is rather high for smectite (> 0.65, values highlighted in bold type, Table 3). These particles may be mixed-layer illite-smectite or illite. Interestingly, the tetrahedral Si is also frequently below the expected values for smectite and within the range of illite or illite-smectite. Alternatively, the high-charge formulas may be due to slight salt contamination (see Cl and S peaks in spectra of Fig. 3). The last formula in the group of the biological freshwater lake experiments is special in that it probably contains Mg in the interlayer, as there is no Na or K. If 0.57 Mg atoms in the formula are assigned to the interlayer space, the octahedral occupancy would be 3. However, there seems to be contamination with a Mg-phase (brucite?) because the tetrahedral occupancy is low, at only 3.90 atoms. The first of the formulas of the inorganic hypersaline water experiments has low octahedral occupancy (1.90). However, this analysis corresponds to the particle in Figure 3b and there is no doubt that this is a phyllosilicate. It is unclear what produced this anomalous result because all other figures in the formula are within expected ranges. Overall, the formulas show a heterogeneous composition. Besides the fact that TEM-AEM data of individual clay frequently show variability, in the present study the chemical variability may be enhanced by the fact that the particles are newly formed and reflect the composition of glass grains from where they formed or include oxide or oxyhydroxide metal contaminants that alter slightly the cation proportions (bottom values of inorganic lake fresh water, and biological and inorganic hypersaline water experiments).

The octahedral composition of the clays in Table 3 was plotted to assess graphically the effect of water chemistry and microbial activity on the composition of the neoformed clay (Fig. 6). The spring and seawater experiments produced very similar clay compositions in both biological and control experiments. The great majority of these clay particles were of dioctahedral type, most of

them within the montmorillonite composition range (Al > Fe, Mg), and some within the beidellite field (Al >> Fe, Mg; Table 3). The experiments with water from the hypersaline and freshwater lakes did show clear and opposite differences between biological and control experiments. Clay particles of biological experiments in hypersaline water had a larger Mg content than the control experiments, whereas in the freshwater lake experiments Mg was less abundant in clay particles from the biological tests.

Discussion

Control on clay composition from glass, water and biological activity

Overall, our results show that glass composition had a large influence on the chemistry of the neoformed clay. The results from experiments with spring and seawater are all similar, with a dominant dioctahedral clay composition, in spite of the very different water chemistry and the abundant microbial mass in the biological tests. A significant proportion of the clay particles in the hypersaline experiments, especially the inorganic experiments, also had a dioctahedral composition, as well as most clay particles from the biological test in the freshwater lake. These results indicate that clay chemistry was controlled by the glass composition, where Al > Fe > Mg, unless water chemistry were somehow "extreme". Such "extreme" composition occurred within the biofilms in the biological hypersaline experiments, where Mg concentration was very high, and in the inorganic freshwater lake experiments, where pH, Mg, and silica concentrations combined to favor formation of Mg-rich clay (as discussed below). Chemical control from the glass existed probably because the major mechanism of clay formation was the in situ transformation of the glass. In such a transformation, Al was more readily available than other octahedral cations (Mg, Fe), because it was more abundant in the transforming glass, even in environments where Mg was very abundant in the solution. Thus, Mg-rich solutions such as those of inorganic hypersaline and seawater experiments did not result in trioctahedral (Mg-rich) clay formation. If clay in our experiments had formed mainly by precipitation from solution, the great majority of hypersaline and seawater clay

362 particles would be of trioctahedral nature, as Al and Fe concentration in solution was negligible as
363 compared to that of Mg. The occurrence of Al-rich clay consistent with smectite of beidellitic
364 composition has been reported frequently in alteration of glass of different chemistries and altered
365 in varying conditions, such as experimental inorganic alteration of rhyolitic tuff (Kawano and
366 Tomita, 1992) and rhyolitic obsidian (Kawano et al., 1993; Kawano and Tomita, 1997), and natural,
367 inorganic alteration of sub-seafloor basaltic glass (Thorseth et al., 2003).
368
369 The observation of silicate particles displaying a continuum in chemical composition from the
370 original glass in two opposite directions, (1) towards cation depletion, and (2) towards dioctahedral
371 clay compositions (Fig. 4), suggests transformations taking place within the glass. Loss of Al, Mg
372 and Fe (as well as Na and K, although not shown in Fig. 4) occurs by leaching or by crystallization
373 of clay within the glass matrix, which latter process produces a depletion of clay-forming cations in
374 surrounding areas of the glass. The crystallization of clay corresponds to the areas of Al-Mg-Fe
375 enrichment. In order to test the existence of this continuum mathematically, a function was fitted to
376 the data points in the spring water results (Fig. 7), where the trend is most clear. The result was a
377 function (of the type $y = a + \{b / [1 + e^{c(x-d)}]\}$) with a high correlation coefficient ($R^2 = 0.97$). The
378 same function was then applied to the other experiments, excluding data with high Mg / (Fe + Al)
379 ratios (hollow dots in Fig. 7). Specifically, values were excluded if (both inequalities need to apply
380 in the two cases): (1) Si / Al+Mg+Fe < 2 and Al / Si < 0.35; (2) Si / Al+Mg+Fe < 4 and Al / Si <
381 0.18. The function was recalculated for each water, allowing the equation coefficients to change.
382 The results were very similar equations with high correlation coefficients (Fig. 7). If clay formation
383 was not produced within the glass, as a result of chemical rearrangements of the elements available
384 in it, there would be no reason for such chemical trends to develop. The existence of a single
385 chemical evolution involving glass, altered glass and dioctahedral clay is strong evidence
386 supporting the in situ transformation of glass into dioctahedral clay.
387

388 The plot using Mg / Si ratios in the x-axis (Fig. 5) generates two clear trends in the spring water
389 experiments, where the data points are tightly concentrated. This can be explained by the facts that
390 (1) all clay particles detected are of dioctahedral composition and thus formed within the clay
391 matrix, and (2) the Mg incorporated into the clay proceeds mainly from the glass because Mg
392 concentration in the water is low (Fig. 1). Magnesium was much more abundant in the other three
393 waters and it contributed much more to the formation of clay, especially of trioctahedral
394 composition. For this reason, their corresponding plots in Figure 5 show no connection between the
395 Mg increase in the neoformed clay, as a horizontal trend, and the vertical trend of the Si /
396 Al+Mg+Fe values. Possibly, many of these particles were formed by precipitation from solution.
397
398 The higher Mg content in the clay from hypersaline biological experiments is explained by the thick
399 microbial biofilm that encapsulated the glass grains and where a high concentration of Mg-rich salt
400 existed (Fig. 2a). Such environment contained so much dissolved Mg that this element may have
401 been sufficiently available to be taken up by the reacting glass in the in situ transformation process,
402 or the high Mg concentration may have promoted clay precipitation from solution. Seawater
403 experiments did not experience Mg-rich clay formation because the biofilm did not enclose the
404 glass grains and there was no Mg enrichment in their proximity. The exponential increase of
405 dissolved Si with time in the experiments (Fig. 1) suggests that precipitation of clay from solution
406 would be more likely towards the end of the experiments, when silica activity was higher. The
407 highest Si concentrations occurred in the hypersaline water. Interestingly, the biological
408 experiments had Si concentrations roughly half of those from the control experiments, which may
409 indicate silica uptake through trioctahedral clay formation within the Mg-rich biofilm environment.
410
411 The fact that Si concentrations in solution increased exponentially with time in three out of the four
412 experiments (Fig. 1) may be explained by the mechanism of in situ transformation of the glass into
413 clay. The increased Si release into solution suggests the creation of a Si-phase more soluble than the

414 glass. Such phase could be the glass itself after atom rearrangement and clay formation, as this
415 transformation would leave parts of the glass depleted from cations and consisting of silica almost
416 exclusively, where silica tetrahedra may form a relatively open framework and/or the residual glass
417 may have a largely increased surface-to-volume ratio, both of which facts would render this residue
418 more soluble. Such phase would be more abundant as the reaction progressed and more clay formed
419 within the glass. The existence of cation-depleted glass is shown in our results (Figs. 4 and 5) but
420 the existence of a residual silica phase of enhanced solubility is only a conjecture.
421
422 The clay composition data from the freshwater lake showed the trend opposite to that of the
423 hypersaline water. The biological experiments with lake fresh water produced mainly dioctahedral
424 clay, and the inorganic experiments produced mainly trioctahedral clay. Because the biological
425 experiments produced results more similar to the majority of the other experiments (i.e., all spring
426 and seawater tests; inorganic test in hypersaline water), the conclusion is that it is the control
427 experiments that behaved in a contrasting manner. The cause of this behaviour in the inorganic
428 experiments must be sought in the lake fresh water, because the water is the only factor different
429 from the other inorganic experiments. Indeed, the original pH of this water (9.00) was the highest
430 (Fig. 1). We explored the possible consequences of pH and water chemistry by assessing cation
431 activities in solution and plotting them on mineral stability diagrams. This was done for the
432 inorganic experiments of the two freshwaters. Comparison of these two cases should indicate the
433 cause for the different behaviour of the freshwater lake tests because, although the two fresh waters
434 had the most similar chemistry, they produced different clay composition. The activities were
435 assessed using the PHREEQC Interactive software. Because anions were measured only in the
436 original solutions, the ion speciation and activity calculations could not be carried out rigorously for
437 the solutions after reaction. We opted for plotting the range of values from ion concentration
438 (measured experimentally) to activity (calculated with PHREEQ) for the original solutions and then
439 assumed that the difference between concentrations and activities would be similar in the solutions

after reaction, which were also plotted. Thus, the assessment provides an approximate range of species activities. Two log [SiO_2] vs. log [$Mg^{2+}/(H^+)^2$] plots were used corresponding to two levels of Al activity (Birsoy, 2002) that are likely to bracket our experimental values (Fig. 8). Saponite is not included in the plots but it would occupy an intermediate position between the talc and montmorillonite fields. The results indicate that the freshwater lake solutions fall closer to or within the trioctahedral phases (talc and saponite), whereas the spring water solutions plot deeper into the montmorillonite field, in agreement with our clay composition data.

However, solution thermodynamics should not be the only control of clay chemistry and cannot explain completely the results of the freshwater experiments from the lake. The reason is that glass composition is an important controlling factor of clay chemistry, and it should be assumed that the glass transformation mechanism producing dioctahedral clay was operating also in these experiments. Thus, in order to generate a clay particle population where trioctahedral clay was most abundant, kinetic effects must have also been important in the inorganic freshwater lake experiments so that trioctahedral clay was generated faster than dioctahedral clay (the latter produced by glass transformation). In fact, kinetic factors would ally with mineral stability factors because the formation rates of trioctahedral smectite are higher than those of dioctahedral smectite (Huertas et al., 2000), especially at surface temperature (Kloprogge et al., 1999). Solutions with activity values within the montmorillonite (dioctahedral) field but next to that of saponite-talc (trioctahedral) will probably produce saponite rather than montmorillonite because of the faster formation rate. The formation of trioctahedral smectite in the inorganic freshwater lake experiments probably took place mainly in the bulk solution but there is evidence from other experiments (Fig. 2b,c) that it also operated at the surface of glass grains or their immediate vicinity. In such process, the competition with dioctahedral clay formation would have been most efficient. The clay in the biological experiments with lake fresh water must have been produced in a similar way in the initial phases of the experiment, i.e., before the biofilm encapsulated the glass grains (open squares in the

466 trioctahedral field in Fig. 6). When the glass was enclosed within the biofilm, however, the water
467 conditions must have changed and slowed down the process of trioctahedral clay production so that
468 dioctahedral clay was finally more abundant (Fig. 6). The most obvious change in local water
469 conditions taking place with the biofilm encapsulation is a pH decrease caused by the usually acidic
470 character of the EPS and by exudation of protons, CO_2 and organic and inorganic acids by the
471 microorganisms (Barker et al., 1997; Valsami-Jones and McEldowney, 2000). Such a local pH
472 decrease would result in conditions further within the montmorillonite stability field (Fig. 8) and in
473 a substantial decrease of the formation rate of trioctahedral clay or perhaps in the suppression of this
474 process.
475
476 **Time effect on chemical controls of the neoformed clay**
477 The results from this study should be placed in the context of the length of the alteration process, as
478 it appears that the neoformed clay composition is dependent on the duration of the alteration. Long-
479 term alteration generally produces clay whose composition is controlled by water chemistry
480 (Cerling et al., 1985) and temperature, for which reason the clay chemistry can record climatic
481 conditions and hydrous regimes (Chamley, 1989). Further to this, studies of smectite composition in
482 bentonite have shown that (1) the chemistry of smectite is linked, with small but measurable
483 variations, to the length of the alteration, causing a drift of the smectite composition with time
484 (Caballero et al., 1992), and (2) similar differences in smectite composition are related to the
485 chemistry of the altering waters (Christidis, 2008). In both studies, the investigated bentonites were
486 completely altered, i.e., they did not represent stages of partially altered volcanic material. Contrary
487 to the above, the chemistry of clay formed at the initial alteration stages of volcanic glass can be
488 largely controlled by rock chemistry, even at high water-rock ratios. Ghiara et al. (1993) used a 25:1
489 water:glass mass ratio in the hydrothermal alteration of basaltic glass, with Al/Mg atomic ratio of
490 ~1.8, by deionized water, which produced saponite, phillipsite and analcime. Analysis of the fluids
491 after the experiments showed them to be in equilibrium with montmorillonite and analcime. Thus,

492 the formation of saponite must have been driven by the chemistry of the glass. Experimental
493 hydrothermal alteration of rhyolitic glass with higher Al/Mg atomic ratio, of ~5, by de la Fuente et
494 al. (2002), using the same water:glass mass ratio and solutions of varying Na/K ratios, produced
495 smectite-rich illite-smectite of montmorillonitic composition. The Al-rich clay product is consistent
496 with the higher Al/Mg ratio in the glass. Besides, the large variation of Na/K ratios in the solution
497 (0.01-100) had no effect on the resulting relative smectite-to-illite ratio, which also suggests glass
498 chemical control on the reaction. In agreement with these results, major glass control on smectite
499 chemistry was reported by Alt and Mata (2000) in submarine basaltic glass alteration where the
500 assessed water:rock mass ratio was ~43. The same appears to be true of the alteration of crystalline
501 silicates. Early weathering of amphibole grains have been reported to produce different clay
502 minerals (Al- or Mg-rich) on different crystallographic cleavage surfaces depending on Mg
503 leachability (i.e., availability to be incorporated in the neoformed clay) on the corresponding surface
504 (Proust et al., 2006). These reports are in agreement with our results and interpretation of a
505 dominant mechanism of in situ glass transformation.
506
507 In contrast to the above, Thomassin et al. (1989) found that the control on the chemical composition
508 of the neoformed clay in experimental alteration of synthetic basaltic glass depended on the
509 water:glass ratio. The experiments reported here also provide examples of the formation of clay
510 controlled by water chemistry (biological hypersaline, inorganic freshwater lake) rather than glass
511 composition. Thus, predominant rock control on alteration of igneous rock to clay may not
512 necessarily be linked to low water:rock ratios as interpreted by some authors (e.g., Giorgetti et al.,
513 2009). Our data and the above discussion indicate kinetic effects as important in determining the
514 relative control on the clay chemistry at least at the first stages of alteration. Atomic rearrangement
515 in the glass appears to be faster than glass dissolution and precipitation for a wide range of water
516 composition. However, water chemistry (pH, Mg concentration) can be such that clay precipitation
517 from solution becomes faster, or the uptake of species by the reacting glass surface is also fast and

incorporates these species into the in situ transformation reaction. Temperature is plausibly another important factor to explore in this connection, linked both with kinetics and thermodynamics, although not discussed here. In the long term, stability conditions take over if water-rock interaction continues. After thorough alteration has taken place, the chemical evolution of the produced clay tends to reflect water composition so that the clay approaches equilibrium with water chemistry.

Microbial effect on clay formation

Our experiments indicate that microorganisms in aquatic environments are efficient controls of the chemistry of neoformed clay by generating biofilms of low permeability that entrap mineral grains and within which biofilms water chemistry can be significantly different from that in the surroundings. The efficiency of biofilms as a chemical barrier from bulk solutions has been demonstrated (Aouad et al., 2006). Water chemistry within biofilms is modified by a number of mechanisms such as cellular activity as discussed above, selective adsorption of cations on organic tissue (Konhauser et al., 1993; Lalonde et al., 2007), possibly by concentration of ions from dissolving entrapped minerals (Staudigel et al., 1995), concentration of solutes from the bulk solution as observed in this study, etc. Even if mineral grains susceptible of alteration are not trapped in the biofilm, the long-term interaction of dissolved species penetrating the biofilms can produce clay precipitation whose composition will probably differ from that of purely inorganic origin in the surrounding environment. This phenomenon is suggested by the common formation of Fe-rich smectite (with a range of Al-Fe composition) within freshwater biofilms (Konhauser and Urrutia, 1999) and nontronite reported within submarine biofilms (Ueshima and Tazaki, 2001). Iron appears to be preferentially adsorbed on microbial walls and EPS fibres, where it reacts with dissolved or colloidal Si and Al to form clays in a catalytic process (Konhauser and Urrutia, 1999; Ueshima and Tazaki, 2001).

543 In nature, the global effectiveness of these biofilms to control the chemistry of the neoformed clays
544 depends on two factors. First, the tightness of the biofilm, because only sufficiently closed systems
545 allow a building up of dissolved species that can modify the clay composition from that which
546 would result from inorganic conditions. This is demonstrated by the absence of biological control in
547 our experiments with seawater, where the biofilm did not enclose the glass grains and they were
548 exposed to altering fluid with the chemistry of the bulk solution, i.e., with no increased or modified
549 ion concentrations. Secondly, the effectiveness of biological control on clay neoformation depends
550 on the continuous reconstruction of the biofilm, by which it traps or covers new, yet unaltered
551 sediment or rock. After the mineral grains in contact with the biofilm have been thoroughly altered
552 the microbial activity will no longer have an effect on clay formation through direct alteration. In
553 such a case, the biofilms could concentrate cations from solution and cause clay precipitation but
554 this process is dependent on the inorganic alteration and dissolution of the rock or sediment, which
555 would then be the main control on clay formation. The question is then whether the dynamics of
556 biofilms is such that they are rebuilt or extended to new areas so that there is a constant turnaround
557 of new unweathered material entrapped within them or, rather, the biofilms are so stable that after
558 some time they encapsulate only the alteration products. In the latter case, the influence of biofilms
559 in the control of clay composition would be limited.
560
561 It was not possible to test whether microbial activity in our experiments accelerated clay formation
562 because the very low clay concentration levels did not allow quantitative analysis (e.g., X-ray
563 diffraction or infra-red spectroscopy). Neither was it possible to produce a visual assessment of the
564 extent of glass weathering using images from the cryo-SEM analysis because much of the surface
565 of glass grains was covered with biofilm, precluding observation. Thus, no evidence could be
566 gathered about possible different clay formation rates in control and biological experiments. It can
567 be speculated that the rate was similar in biological and control experiments where the mechanism
568 of clay formation was the same (in situ glass alteration) and the range of clay composition was very

similar, as in the spring and seawater tests. For the hypersaline and freshwater lake waters, where more than one mechanism of clay formation may have operated, and where the composition of the clay was different between control and biological experiments, clay formation rates may have also differed. As indicated above, Mg-rich trioctahedral smectite crystallizes faster than Al-, dioctahedral smectite. The issue of biological modification of clay formation rate is important to assess large-scale geochemical effects of biological activity. Many authors sustain that, overall, biota accelerates mineral weathering (Barker et al., 1997), which should, in principle, result in accelerated clay formation (Kennedy et al., 2006). Evidence exists for faster silicate dissolution induced by microorganisms but there is no observation of a concomitant accelerated clay formation (Thorseth et al., 1995; Staudigel et al., 1995; Ullman et al., 1996; Barker et al., 1998; Song et al., 2007; Balogh-Brunstad et al., 2008). It needs also to be considered that microbial mats may have long-term effects of reduction of mineral weathering by protecting mineral surfaces with layers of stable, secondary minerals and biological material (Staudigel et al., 1995). Further investigation is needed to assess biological effects on clay formation rates.

Acknowledgments

We thank T. Wing-Dudek for her contribution in the planning of the experiments, V. Dekov and E. Neykova for providing the volcanic glass, F. Pinto for his expert technical support in the cryo-SEM study, and W. Huff and an anonymous reviewer for their comments that helped to improve the clarity of the manuscript. This work was funded by the Marie Curie Fellowship programme, project Bio-Clays (2009-2011).

592 **References**

593

594 Abdelouas, A., Crovisier, J., Lutze, W., Fritz, B., Mosser, A., and Müller, R. (1994) Formation of
595 hydrotalcite-like coumpounds during R7T7 nuclear waste glass and basaltic glass alteration. Clays
596 and Clay Minerals, 42, 526-533.

597

598 Alt, J.C. and Mata, P. (2000) On the role of microbes in the alteration of submarine basaltic glass: a
599 TEM study. Earth and Planetary Science Letters, 181, 301-313.

600

601 Aouad, G., Geoffroy, V.A., Crovisier, J.L., Meyer, J.M., Damidot, D., and Stille P. (2006) The role
602 of biofilms on the alteration kinetics of waste matrices. Geophysical Research Abstracts, 8, 08580.

603

604 Balogh-Brunstad, Z., Keller, C.K., Dickinson, J.T., Stevens, F., Li, C.Y., and Bormann, B.T. (2008)
605 Biotite weathering and nutrient uptake by ectomycorrhizal fungus, Suillus tomentosus, in liquid-
606 culture experiments. Geochimica et Cosmochimica Acta, 72, 2601-2618.

607

608 Barker, W.W. and Banfield, J.F. (1996) Biologically versus inorganically mediated weathering
609 reactions: relationships between minerals and extracellular microbial polymers in lithobiontic
610 communities. Chemical Geology, 132, 55-69.

611

612 Barker, W.W., Welch, S.A., and Banfield, J.F. (1997) Biogeochemical weathering of silicate
613 minerals. In J.F. Banfield and K.H. Nealson, Eds., Geomicrobiology: Interactions Between
614 Microbes and Minerals, 35, p. 391-428. Reviews in Mineralogy, Mineralogical Society of America,
615 Washington D.C.

616

617 Barker, W.W., Welch, S.A., Chu, S., and Banfield, J.F. (1998) Experimental observations of the
618 effects of bacteria on aluminosilicate weathering. American Mineralogist, 83, 1551-1563.
619
620 Birsoy, R. (2002) Formation of sepiolite-palygorskite and related minerals from solution. Clays and
621 Clay Minerals, 50, 736-745.
622
623 Brownlow, A.H. (1996) Geochemistry, 580 p. Prentice Hall, New Jersey.
624
625 Caballero, E., Reyes, E., Delgado, A., Huertas, F., and Linares, J. (1992) The formation of
626 bentonite: mass balance effects. Applied Clay Science, 6, 265-276.
627
628 Cerling, T., Brown, F., and Bowman J. (1985) Low-temperature alteration of volcanic glass:
629 hydration, Na, K, ^{18}O and Ar mobility. Chemical Geology (Isotope Geoscience), 52, 281-293.
630
631 Chamley, H. (1989) Clay Sedimentology, 623 p. Springer-Verlag, Berlin.
632
633 Chorover, J., Kretzschmar, R., Garcia-Pichel, F., and Sparks, D.L. (2006) Soil biogeochemical
634 processes within the critical zone. Elements, 3, 321-326.
635
636 Christidis, G. (2008) Do bentonites have contradictory characteristics? An attempt to answer
637 unanswered questions. Clay Minerals, 43, 515-529.
638
639 Cuadros, J. (2012) Clay crystal-chemical adaptability and transformation mechanisms. Clay
640 Minerals, 47, 147-164. doi 10.1180/claymin.2012.047.2.01
641

642 de la Fuente, S., Cuadros, J., Fiore, S., and Linares, J. (2000) Electron microscopy study of volcanic
643 tuff alteration to illite-smectite under hydrothermal conditions. Clays and Clay Minerals, 48, 339-
644 350.
645
646 de la Fuente, S., Cuadros, J., and Linares, J. (2002) Early stages of volcanic tuff alteration in
647 hydrothermal experiments: Formation of mixed-layer illite-smectite. Clays and Clay Minerals, 50,
648 578-590.
649
650 Deocampo, D., Cuadros, J., Wing-Dudek, T., Olives, J., and Amouric, A. (2009) Saline lake
651 diagenesis as revealed by coupled mineralogy and geochemistry of multiple ultrafine clay phases:
652 Pliocene Olduvai gorge, Tanzania. American Journal of Science, 309, 834-868, DOI
653 10.2475/09.2009.03.
654
655 Ehrlich, H.L. (1998) Geomicrobiology: its significance for geology. Earth-Science Reviews, 45, 45-
656 60.
657
658 Fiore, S., Huertas, F.J., Huertas, F., and Linares, J. (2001) Smectite formation in rhyolitic obsidian
659 as inferred by microscopic (SEM-TEM-AEM) investigation. Clay Minerals, 36, 489-500.
660
661 Ghiara, M.R., Franco, E., Petti, C., Stanzione, D., and Valentino, G.M. (1993) Hydrothermal
662 interaction between basaltic glass, deionized water and seawater. Chemical Geology, 104, 125-138.
663
664 Giorgetti, G., Monecke, T., Kleeberg, R., and Hannington, M. (2009) Low-temperature
665 hydrothermal alteration of Trachybasalt at Conical Samount, Papua New Guinea: formation of
666 smectite and metastable precursor phases. Clays and Clay Minerals, 57, 725-741.
667

668 Graham, L.E. and Wilcox, L.W. (2000). Algae, 640 p. Prentice-Hall, Upper Saddle River, New
669 Jersey.
670
671 Huertas, F.J., Cuadros, J., Huertas, F., and Linares, J. (2000) Experimental study of the
672 hydrothermal formation of smectite in the beidellite-saponite series. American Journal of Science,
673 300, 504-527.
674
675 John, D.M., Whitton, B.A., and Brook A.J., Eds. (2002) The freshwater algal flora of the British
676 Isles: an identification guide to freshwater and terrestrial algae, 714 p. Cambridge University Press,
677 Cambridge, UK.
678
679 Kawano, M. and Tomita, K, (1992) Formation of allophane and beidellite during hydrothermal
680 alteration of volcanic glass below 200 ºC. Clays and Clay Minerals, 40, 666-674.
681
682 Kawano, M., Tomita, K., and Kamino, Y. (1993) Formation of clay minerals during low
683 temperature experimental alteration of obsidian. Clays and Clay Minerals, 41, 431-441.
684
685 Kawano, M. and Tomita, K. (1997) Experimental study on the formation of zeolites from obsidian
686 by interaction with NaOH and KOH solutions at 150 and 200 ºC. Clays and Clay Minerals, 45, 365-
687 377.
688
689 Kennedy, M., Droser, M., Mayer, L.M., Pevear D., and Mrofka, D. (2006) Late Precambrian
690 oxygenation; inception of the clay mineral factory. Science, 311, 1446-1449.
691
692 Kloprogge, J., Komarneni, S., and Amonette, J. (1999) Synthesis of smectite clay minerals: a
693 critical review. Clays and Clay Minerals, 47, 529-554.

694

695 Konhauser, K., Fyfe, W., Ferris, F., and Beveridge, T. (1993) Metal sorption and mineral
696 precipitation by bacteria in two Amazonian river systems: Rio Solimões and Rio Negro, Brazil.
697 Geology, 21, 1103-1106.

698

699 Konhauser, K. and Urrutia, M. (1999) Bacterial clay authigenesis: a common biogeochemical
700 process. Chemical Geology, 161, 399-413.

701

702 Lalonde, S.V., Amskold, L.A., Warren, L.A., and Konhauser, K.O. (2007) Surface chemical
703 reactivity and metal adsorptive properties of natural cyanobacterial mats from an alkaline
704 hydrothermal spring, Yellowstone National Park. Chemical Geology, 243, 36-52.

705

706 Proust, D., Caillaud, J., and Fontaine, C. (2006) Clay minerals in early amphibole weathering : tri-
707 to dioctahedral sequence as a function of crystallization sites in the amphibole. Clays and Clay
708 Minerals, 54, 351-362.

709

710 Sánchez-Navas, A., Martín-Algarra, A., and Nieto, F. (1998) Bacterially-mediated authigenesis of
711 clays in phosphate stromatolites. Sedimentology, 45, 519-533.

712

713 Song, W., Ogawa, N., Oguchi, C.T., Hatta, T., and Matsukura, Y. (2007) Effect of Bacillus subtilis
714 on granite weathering: A laboratory experiment. Catena, 70, 275-281.

715

716 Staudigel, H., Chastain, R., Yayanos, A., and Bourcier, W. (1995) Biologically mediated
717 dissolution of glass. Chemical Geology, 126, 147-154.

718

719 Tazaki, K. (2005) Microbial formation of a halloysite-like mineral. Clays and Clay Minerals, 53,
720 224-233.
721
722 Thomassin, J.-H., Boutonnat, F., Touray, J.-C., and Baillif P. (1989) Geochemical role of the
723 water/rock ratio during the experimental alteration of a synthetic basaltic glass at 50°C. An XPS
724 and STEM investigation. European Journal of Mineralogy, 1, 261-274.
725
726 Thompson, M. and Walsh, J.N. (2003) Handbook of Inductively Coupled Plasma Atomic Emission
727 Spectrometry, 316 p. Viridian, Woking, UK.
728
729 Thorseth, I.H., Furnes, H., and Tumyr, O. (1995) Textural and chemical effects of bacterial activity
730 on basaltic glass: an experimental approach. Chemical Geology, 119, 139-160.
731
732 Thorseth, I.H., Pedersen, R.B., and Christie, D.M. (2003) Microbial alteration of 0–30-Ma seafloor
733 and sub-seafloor basaltic glasses from the Australian Antarctic Discordance. Earth and Planetary
734 Science Letters, 215, 237-247.
735
736 Ueshima, M. and Tazaki, K. (2001) Possible role of microbial polysaccharides in nontronite
737 formation. Clays and Clay Minerals, 49, 292-299.
738
739 Ullman, W.L., Kirchman, D.L., Welch, S.A., and Vandevivere, P. (1996) Laboratory evidence for
740 microbially mediated silicate mineral dissolution in nature. Chemical Geology, 132, 11-17.
741
742 Urrutia, M.M. and Beveridge, T.J. (1994) Formation of fine-grained metal and silicate precipitates
743 on a bacterial surface (Bacillus subtilis). Chemical Geology, 116, 261-280.
744

745 Valsami-Jones, E. and McEldowney, S. (2000) Mineral dissolution by heterotrophic bacteria:
746 principles and methodologies. In J.D. Cotter-Howells, L.S. Campbell, E. Valsami-Jones and M.
747 Batchelder, Eds., Environmental Mineralogy: Microbial Interactions, Anthropogenic Influences,
748 Contaminated Land and Waste Management, 9, p. 27-55. The Mineralogical Society Series,
749 London, UK.

750

751

752 Figure captions

753

754 Figure 1. Plots of cation concentrations and pH values of the original waters (black triangles) and
755 those after several reaction periods, for inorganic (controls) and biological experiments. There are
756 three replicas of the 18-month experiments. Uncertainty of cation concentrations is ±0.1-10% (σ) of
757 the value, depending on element concentration. Uncertainty of pH is ±0.02 (σ).

758

759 Figure 2. Cryo-SEM images of biofilm and glass grains, and EDX spectra of some specific area. In
760 panels (b) and (c) the EDX results are shown numerically for space sake. The results are the
761 integration of the peak areas normalized to Si 100. (a) Back-scattered electron image from a
762 hypersaline water experiment of a pristine glass grain (grain with smooth surface) embedded in
763 crystallized salt (area with a pattern of cavities) from the brine within the biofilm. The EDX spectra
764 taken in numerous spots of the patterned surface indicates sulphate and chloride of Na and Mg. The
765 round structure to the left of the glass grain is probably a cell. (b) Back-scattered electron image of
766 a glass grain partially covered with a thin film of biological origin (slightly darker contrast area on
767 the left) from one of the hypersaline lake experiments. Most of the glass shows no alteration
768 (spectrum from spot 1) and a smooth surface. The upper zone in the central shallow cavity (spot 2)
769 shows a rough surface and increased Mg concentration that was usually diagnostic of chemical
770 alteration. Unfortunately, Fe information in these spectra was lost (na: not available). (c) Secondary
771 electron image from one of the spring water experiments of a glass grain with signs of alteration.
772 The smooth surface corresponds to unaltered glass (spot 1). Two areas developed roughness and
773 had clearly different chemical composition from the glass, with increased Mg and Fe, and Si /
774 Al+Fe+Mg ratios approaching those of clay (spots 2 and 3). (d) Detail of a glass grain from one of
775 the hypersaline water experiments, showing platy particles developing on the surface of the glass.

776

Figure 3. TEM image and AEM spectra of particles with smectite morphology and clay-like composition from the experimental products. (a) Large grain of K-rich clay of beidellitic composition, from one of the 18-month control experiments with spring water. The thin films (top, right) and thick grain (very dark contrast) have the same composition; the white dots indicate two of the spots that were analyzed and produced almost identical AEM spectra. The sharp outline and thickness of the particle suggests in situ chemical transformation of a glass grain. The areas with light gray contrast in the background correspond to the Formvard film on the Cu grid, and the white round areas resembling bubbles are holes in the film. (b) Small particle of a phyllosilicate as indicated by the sharp hexagonal SAED pattern and chemical composition; from one of the 18-month biological hypersaline water experiments. (c) Group of particles from one of the control seawater experiments. The large particle at the top (1) and small one at the bottom (2) have a clay-like composition of beidellitic character. Other particles in the area indicated the presence of non-silicate phases.

Figure 4. Plots of Al / Si vs. Si / Al+Mg+Fe ratios in silicate particles from TEM-AEM data. The data points include glass, altered glass and clay particles. The approximate composition of the original glass is indicated by the circumference. These data provide a general view of the chemical trends in the glass alteration during the experiments. The clay particles are approximately identified by having a Si / Al+Mg+Fe ratio between 1 and 2 (see text). The four fields within the range $2 \geq$ Si / Al+Mg+Fe ≥ 1, from nontronite/saponite to kaolinite (as indicated below the fields), are only intended as an approximate assessment of the chemical characteristics of the clay.

Figure 5. Plots of Mg / Si vs. Si / Al+Mg+Fe ratios in silicate particles from TEM-AEM data. The original glass composition is marked by a circumference. The horizontal lines mark the clay fields as in Figure 4, divided in two approximate fields: dioctahedral (nontronite, montmorillonite,

802 beidellite and kaolinite) and saponite (trioctahedral). Notice that the x-axes have different ranges in
803 the several plots.
804
805 Figure 6. Plots of octahedral Mg vs. octahedral Al+Fe from the TEM-AEM analyses of clay
806 particles formed during the reactions. The lines delimit the approximate fields of smectite
807 composition: trioctahedral (Mg-rich), particles of mixed dioctahedral and trioctahedral composition
808 (single particles of intermediate composition or mixed particles of both types), and dioctahedral
809 (Al-,Fe-rich).
810
811 Figure 7. Plots of Al / Si vs. Si / Al+Mg+Fe ratios in silicate particles from TEM-AEM data, as in
812 Fig. 4. In the present figure, the data points that appear to fall within a continuous chemical trend of
813 glass transformation that leads from the original glass composition towards the formation of
814 dioctahedral clay (lower part of the curve) and towards Al-Mg-Fe-depleted glass (higher part of the
815 curve) are represented as black dots ("Transf" data points). The data points outside this trend are
816 represented by hollow dots ("Other") and correspond to trioctahedral clay formation or glass
817 alteration towards it.
818
819 Figure 8. Log-log plots of species concentrations or activities from the solutions corresponding to
820 the two fresh waters, in the control experiments. Activities could only be calculated for the original
821 water samples (see text). The difference between log of the activity and of the experimentally
822 measured concentration in the original waters was assumed to be the same in all the others. The data
823 points correspond to the experimental concentrations and the edge of the bars provide the activity
824 values. The stability fields are from the literature (Birsoy, 2002) calculated for the following
825 activity ratios: log $[Al / H^3] = 8.5$ (a) and 7.5 (b), which values are likely to bracket the conditions
826 in our freshwater experiments (log $[Al / H^3] = 8.35$ corresponds to pyrophyllite and quartz
827 saturation; log $[Al / H^3] = 7.2$ corresponds to kaolinite and pyrophyllite saturation). The saponite

828 field would be between those of talc and montmorillonite. The data show that most experiments
829 from the lake water plot within or closer to the trioctahedral field, which is consistent with these
830 experiments producing mainly trioctahedral smectite (see text). The time arrows indicate the
831 increasing duration of the experiments from 0 to 18 months; i.e., silica concentration increased with
832 time.
833

834

835 Table 1. Chemical composition of the volcanic glasses and their mixture (Lipari/Milos = 3.34 in

836 wt.) used in the experiments.

	SiO_2 (wt%)	Al_2O_3 (wt%)	$Fe_2O_3^*$ (wt%)	MgO (wt%)	TiO_2 (wt%)	MnO (wt%)	CaO (wt%)	Na_2O (wt%)	K_2O (wt%)	P_2O_5 (wt%)	Total (wt%)	Ba (ppm)	Sr (ppm)
Lipari	76.9	11.9	3.63	0.111	0.252	0.106	1.67	4.28	2.83	<0.1	101.7	545	93.2
Milos	78.6	12.8	1.10	0.213	0.166	0.062	1.31	3.90	3.56	<0.1	101.8	510	93.6
Mixture	73.2	12.9	3.28	0.130	0.252	0.100	1.99	4.43	3.24	<0.1	99.5	580	105.0

837 * Total Fe as Fe_2O_3.

838 Analytical errors are ±0.2-2.5 % (σ) of the measured values.

839

840

841 Table 2. Microbial fauna in the original waters and glass and at two stages of the experiments, as

842 identified by DNA analyses (bacteria and fungi) and optical microscopy (algae and cyanobacteria).

843 The room ambient was investigated during the experiments.

	Bacteria		
	Original	6 months	14 months
Freshwater lake	Betaproteobacteria Acidovorax sp. Sphingomonas sp. Brevundimonas sp. Acinetobacter sp.	Betaproteobacteria Acidovorax sp. Sphingomonas sp. Brevundimonas sp. Acinetobacter sp. Micrococcus sp.	Betaproteobacteria Sphingomonas sp. Brevundimonas sp.
Spring water	Pseudomonas sp. (grey-green) Acidovorax sp. Sphingomonas sp. Brevundimonas sp. Pseudomonas sp. (white) Pseudomonas mendocina	 Sphingomonas sp. Brevundimonas sp. Burkholderiales sp. Granulocystopsis decorata (cyanobacterium)	 Sphingomonas sp. Brevundimonas sp. Burkholderiales sp.
Seawater	Actinobacteria? Marinobacter sp. Salinibacterium amurskyense Pseudoalteromonas sp. (white) Olleya sp. Pseudoalteromonas haloplanktis (orange) Brevundimonas sp.	 Salinibacterium amurskyense Micrococcus luteus Microcoleus or Hydrocoleum sp. (cyanobacteria)	 Salinibacterium amurskyense Micrococcus luteus
Hypersaline	Halomonas alkaliphila Pseudoalteromonas sp. Pseudomonas sp.	Halomonas alkaliphila Pseudoalteromonas sp. Pseudomonas sp. Micrococcus sp. (luteus?) Bosea thiooxidans	 Micrococcus sp. (luteus?)
Volcanic glass Room ambient	Bacillus sp. (grey) Burkholderiales bacterium Arthrobacter sp. Kocuria palustris Bacillus sp. (white)		
	Fungi		
Freshwater lake		White, unidentified Black-green, unidentified	White, unidentified Aspergillus sclerotiorum
Spring water		White, unidentified Black-brown, unidentified	Tritirachium sp.
Seawater		Ascomycota sp. Cadophora malorum Black-green, unidentified	Ascomycota sp.
Hypersaline		White, unidentified Black, unidentified	White, unidentified Penicillium sp.
Volcanic glass			
Room ambient	Black, unidentified Dark green, unidentified Brown, unidentified		

	Algae and cyanobacteria		
Freshwater lake	Chlorella Chaetopeltis orbicularis	Chlorella Chaetopeltis orbicularis Anabaena Heribaudiella fluviatilis?	Chaetopeltis orbicularis Anabaena Heribaudiella fluviatilis? Microcystis? Klebsormidium or Tolypothrix
Spring water	Microcystis Chlorokybus	Microcystis Chlorokybus Chlorella saccaharophila or ellipsoidea	Microcystis Klebsormidium dissectum Heterococcus chodatii? Anabaena Chaetopeltis orbicularis Heribandiella fluvialis? Microcystis?
Seawater	Anabaena Chlorella	Chlorella Navicula gregaria? Navicula abrupta? Skeletonema? Melosira nummoloides? Dinoflagellate	 Navicula gregaria? Navicula abrupta? Skeletonema? Melosira nummoloides? Amphora tenerrima Colourless, featureless colony
Hypersaline	Cylindrospermopsis?[a] Tolypothrix?[a] Chlorella Navicula capitoradiata? Navicula humii Hustedt? Navicula hyalinula?	 Chlorella Navicula capitoradiata?	Cylindrospermopsis?[a] Chlorella? Microcystis[b]
Volcanic glass			
Room ambient			

[a] Freshwater species according to Graham and Wilcox (2000), although John et al. (2002) indicate that they also live on mineral and plant surfaces, where water may be solute-saturated.

[b] Mainly freshwater species but *Microcystis aeruginosa* can live in moderately brackish waters (John et al., 2002).

Table 3. Structural formulas of 2:1 phyllosilicate particles from TEM-AEM analyses calculated on the basis of $O_{10}(OH)_2$. Within each sample, the formulas are arranged with increasing octahedral occupancy. The figures that have unusual values for smectite are highlighted in bold. They correspond mainly to a high layer charge (> 0.65) that may be due to clay of illitic nature or the result of K-Na contamination from salt.

	Si_{tet}	Al_{tet}	Al_{oct}	Mg_{oct}	Fe_{oct}	K_{int}	Na_{int}	Sum tet	Sum Oct	Layer ch
Freshwater	3.65	0.35	1.99	0.00	0.00	0.00	0.38	4.00	1.99	0.38
lake	3.69	0.31	1.86	0.05	0.11	0.10	0.20	4.00	2.02	0.30
Biological	3.20	0.80	1.46	0.19	0.39	0.49	0.39	4.00	2.04	**0.88**
	3.77	0.23	0.84	0.43	0.83	0.28	0.11	4.00	2.09	0.38
	3.30	0.70	1.90	0.01	0.22	0.30	0.00	4.00	2.14	0.30
	3.50	0.50	0.51	0.41	1.24	0.37	0.04	4.00	2.16	0.41
	3.10	0.90	2.03	0.15	0.00	0.32	0.20	4.00	2.18	0.52
	3.05	0.95	1.63	0.19	0.37	0.32	0.24	4.00	2.19	0.56
	3.16	0.84	1.72	0.22	0.31	0.00	0.32	4.00	2.25	0.32
	3.34	0.66	0.97	0.51	0.80	0.21	0.12	4.00	2.28	0.32
	3.58	0.42	0.54	1.58	0.33	0.00	0.66	4.00	2.45	**0.66**
	3.32	0.68	0.66	1.29	0.56	0.31	0.11	4.00	2.51	0.43
	3.34	0.66	0.20	2.08	0.52	0.13	0.23	4.00	2.79	0.36
	3.86	0.14	0.01	2.99	0.04	0.00	0.01	4.00	3.04	0.01
	3.84	0.14	0.00	3.02	0.05	0.02	0.04	3.97	3.07	0.05
	3.13	**0.77**	**0.00**	**3.55**	**0.02**	**0.00**	**0.00**	**3.90**	**3.57**	**0.00**
Freshwater	3.20	0.80	1.90	0.08	0.04	0.32	0.49	4.00	2.02	**0.81**
lake	3.98	0.02	0.87	1.35	0.21	0.07	0.00	4.00	2.43	0.07
Inorganic	3.61	0.39	0.93	1.15	0.36	0.12	0.11	4.00	2.44	0.24
	3.76	0.24	0.39	1.37	0.73	0.00	0.15	4.00	2.48	0.15
	3.81	0.19	0.71	1.43	0.37	0.06	0.00	4.00	2.52	0.06
	3.62	0.38	0.82	1.76	0.00	0.00	0.41	4.00	2.58	0.41
	3.64	0.36	0.98	1.41	0.19	0.00	0.02	4.00	2.58	0.02
	3.71	0.29	0.55	1.80	0.31	0.11	0.00	4.00	2.66	0.11
	3.82	0.18	0.55	1.99	0.16	0.07	0.00	4.00	2.70	0.07
	3.60	0.40	0.43	1.78	0.51	0.00	0.02	4.00	2.72	0.02
	3.46	0.54	0.88	1.81	0.08	0.04	0.00	4.00	2.77	0.04
	3.96	0.04	0.13	2.59	0.15	0.00	0.00	4.00	2.88	0.00
	3.84	0.16	0.18	2.55	0.17	0.00	0.03	4.00	2.89	0.03
	3.77	0.23	0.09	2.73	0.16	0.00	0.02	4.00	2.98	0.02
	3.81	0.16	0.00	2.89	0.16	0.00	0.04	**3.97**	**3.05**	0.04
Spring water	3.85	0.15	1.28	0.36	0.33	0.26	0.33	4.00	1.97	0.59
Biological	3.22	0.78	1.76	0.18	0.11	0.77	0.03	4.00	2.06	**0.80**
	3.53	0.47	1.49	0.33	0.26	0.40	0.18	4.00	2.07	0.58
	3.62	0.38	1.40	0.40	0.28	0.38	0.16	4.00	2.08	0.54
	3.64	0.36	1.23	0.40	0.45	0.27	0.23	4.00	2.08	0.50
	3.44	0.56	1.53	0.27	0.29	0.55	0.02	4.00	2.09	0.57
	3.51	0.49	1.29	0.41	0.41	0.21	0.37	4.00	2.11	0.58
	3.57	0.43	1.27	0.47	0.41	0.35	0.12	4.00	2.14	0.48
	3.43	0.57	1.46	0.45	0.25	0.33	0.23	4.00	2.15	0.56
	3.54	0.46	1.42	0.40	0.35	0.29	0.07	4.00	2.17	0.36

	3.26	0.74	1.32	0.49	0.41	0.33	0.23	4.00	2.22	0.55
	3.44	0.56	1.14	0.66	0.47	0.30	0.12	4.00	2.27	0.41
	3.29	0.71	1.39	0.63	0.27	0.37	0.13	4.00	2.28	0.50
	3.42	0.58	1.11	0.69	0.48	0.24	0.19	4.00	2.28	0.43
	3.29	0.71	1.19	0.56	0.54	0.33	0.07	4.00	2.29	0.40
	3.26	0.74	1.29	0.64	0.37	0.24	0.24	4.00	2.30	0.48
	3.25	0.75	1.05	0.80	0.49	0.37	0.17	4.00	2.34	0.54
	3.18	0.82	0.93	0.64	0.78	0.29	0.11	4.00	2.35	0.40
	3.27	0.73	1.21	0.75	0.40	0.29	0.10	4.00	2.36	0.40
	3.25	0.75	0.91	0.79	0.67	0.34	0.09	4.00	2.37	0.43
	3.21	0.79	1.03	0.89	0.51	0.24	0.13	4.00	2.44	0.37
	3.25	0.75	0.94	1.26	0.35	0.24	0.14	4.00	2.54	0.38
Spring water	3.15	0.85	1.69	0.13	0.22	0.79	0.09	4.00	2.03	**0.88**
Inorganic	3.12	0.88	1.68	0.13	0.23	0.83	0.08	4.00	2.03	**0.91**
	3.11	0.89	1.69	0.12	0.23	0.82	0.08	4.00	2.04	**0.90**
	3.14	0.86	1.70	0.12	0.22	0.77	0.09	4.00	2.04	**0.86**
	3.70	0.30	1.37	0.36	0.36	0.41	0.00	4.00	2.08	0.41
	3.71	0.29	1.43	0.37	0.29	0.35	0.03	4.00	2.09	0.38
	3.28	0.72	1.53	0.27	0.31	0.55	0.13	4.00	2.10	**0.67**
	3.09	0.91	1.96	0.09	0.05	0.37	0.32	4.00	2.10	**0.69**
	3.20	0.80	1.74	0.24	0.12	0.56	0.15	4.00	2.11	**0.72**
	3.63	0.37	1.37	0.42	0.34	0.34	0.07	4.00	2.12	0.42
	3.54	0.46	1.29	0.43	0.41	0.32	0.19	4.00	2.13	0.51
	3.38	0.62	1.53	0.36	0.24	0.50	0.08	4.00	2.13	0.58
	3.19	0.81	1.53	0.15	0.47	0.28	0.22	4.00	2.15	0.50
	3.62	0.38	1.32	0.44	0.43	0.26	0.02	4.00	2.18	0.28
	3.40	0.60	1.36	0.49	0.36	0.31	0.15	4.00	2.21	0.45
	3.41	0.59	1.18	0.59	0.46	0.35	0.17	4.00	2.22	0.52
	3.22	0.78	1.73	0.27	0.22	0.21	0.18	4.00	2.22	0.39
	3.32	0.68	1.50	0.43	0.32	0.29	0.10	4.00	2.24	0.38
	3.19	0.81	1.38	0.52	0.46	0.19	0.08	4.00	2.35	0.28
	3.19	0.81	0.83	0.84	0.70	0.39	0.13	4.00	2.38	0.52
Seawater	3.21	0.79	1.72	0.16	0.12	0.89	0.02	4.00	2.01	**0.92**
Biological	3.22	0.78	1.70	0.18	0.13	0.90	0.02	4.00	2.01	**0.92**
	3.56	0.44	1.60	0.24	0.24	0.41	0.05	4.00	2.07	0.47
	3.30	0.70	1.56	0.27	0.26	0.70	0.02	4.00	2.08	**0.72**
	3.45	0.55	1.55	0.33	0.21	0.54	0.05	4.00	2.10	0.59
	3.08	0.92	1.89	0.16	0.06	0.61	0.14	4.00	2.11	**0.74**
	3.30	0.70	1.62	0.28	0.22	0.53	0.10	4.00	2.11	0.64
	3.44	0.56	1.41	0.38	0.33	0.43	0.14	4.00	2.12	0.58
	3.53	0.47	1.50	0.34	0.29	0.31	0.13	4.00	2.12	0.45
	3.52	0.48	0.83	0.75	0.58	0.28	0.48	4.00	2.15	**0.76**
	3.51	0.49	1.47	0.42	0.27	0.34	0.10	4.00	2.16	0.44
	3.50	0.50	1.19	0.65	0.34	0.36	0.25	4.00	2.18	0.61
	3.57	0.43	1.35	0.49	0.36	0.25	0.08	4.00	2.20	0.33
	3.48	0.52	1.34	0.53	0.33	0.33	0.12	4.00	2.20	0.45
	3.50	0.50	1.10	0.64	0.50	0.34	0.08	4.00	2.24	0.42
	3.40	0.60	1.36	0.51	0.38	0.35	0.00	4.00	2.25	0.35
	3.33	0.67	1.22	0.61	0.48	0.27	0.10	4.00	2.31	0.37
	3.41	0.59	1.23	0.74	0.34	0.23	0.17	4.00	2.31	0.40
	3.30	0.70	0.98	0.75	0.58	0.44	0.06	4.00	2.32	0.50
	3.21	0.79	1.35	0.69	0.33	0.31	0.05	4.00	2.37	0.35

	3.41	0.59	0.83	1.13	0.47	0.24	0.18	4.00	2.43	0.42
Seawater	3.17	0.83	1.85	0.11	0.06	0.27	0.60	4.00	2.02	**0.87**
Inorganic	3.21	0.79	1.02	0.59	0.45	0.52	0.70	4.00	2.06	**1.21**
	3.27	0.73	1.71	0.20	0.15	0.33	0.41	4.00	2.06	**0.74**
	3.25	0.75	1.68	0.24	0.16	0.64	0.11	4.00	2.08	**0.76**
	3.38	0.62	1.59	0.35	0.15	0.64	0.06	4.00	2.09	**0.70**
	3.33	0.67	1.66	0.27	0.16	0.62	0.05	4.00	2.09	**0.67**
	3.28	0.72	1.45	0.41	0.25	0.44	0.38	4.00	2.10	**0.82**
	3.30	0.70	1.41	0.39	0.32	0.54	0.17	4.00	2.12	**0.72**
	3.59	0.41	1.07	0.69	0.37	0.67	0.04	4.00	2.13	**0.71**
	3.43	0.57	1.33	0.50	0.31	0.43	0.21	4.00	2.14	0.64
	3.46	0.54	1.33	0.48	0.33	0.31	0.27	4.00	2.15	0.59
	3.46	0.54	1.40	0.50	0.25	0.44	0.13	4.00	2.16	0.57
	3.19	0.81	1.77	0.30	0.09	0.49	0.14	4.00	2.16	0.62
	3.54	0.46	1.49	0.54	0.14	0.45	0.05	4.00	2.17	0.50
	3.23	0.77	1.51	0.45	0.22	0.51	0.17	4.00	2.18	**0.68**
	3.31	0.69	1.40	0.57	0.20	0.57	0.14	4.00	2.18	**0.71**
	3.53	0.47	1.23	0.66	0.33	0.29	0.17	4.00	2.22	0.46
	3.26	0.74	1.00	0.85	0.44	0.37	0.33	4.00	2.30	**0.70**
	3.43	0.57	1.09	0.87	0.35	0.40	0.10	4.00	2.31	0.50
	3.32	0.68	0.85	1.00	0.47	0.33	0.38	4.00	2.33	**0.70**
	3.29	0.71	0.87	0.85	0.64	0.27	0.23	4.00	2.36	0.49
Hypersaline	3.83	0.17	1.46	0.07	0.48	0.00	0.22	4.00	2.01	0.22
Biological	3.33	0.67	1.78	0.26	0.10	0.30	0.21	4.00	2.14	0.51
	3.34	0.66	1.29	0.71	0.25	0.44	0.20	4.00	2.25	0.64
	3.39	0.61	1.15	0.86	0.29	0.18	0.39	4.00	2.30	0.58
	3.24	0.76	1.07	0.76	0.49	0.26	0.30	4.00	2.32	0.56
	3.45	0.55	1.00	1.01	0.31	0.29	0.31	4.00	2.32	0.60
	3.31	0.69	0.85	1.53	0.23	0.30	0.09	4.00	2.61	0.39
	3.12	0.88	0.57	1.90	0.25	0.21	0.43	4.00	2.72	0.63
	3.70	0.30	0.08	2.49	0.30	0.00	0.17	4.00	2.87	0.17
	3.28	0.72	0.55	1.99	0.34	0.07	0.00	4.00	2.88	0.07
	3.62	0.38	0.27	2.49	0.17	0.10	0.00	4.00	2.92	0.10
	3.57	0.43	0.15	2.64	0.17	0.11	0.11	4.00	2.95	0.22
	3.26	0.74	0.01	3.03	0.07	0.06	0.40	4.00	**3.10**	0.46
	3.24	0.76	0.03	2.99	0.11	0.14	0.20	4.00	**3.14**	0.34
	3.52	0.33	0.00	3.23	0.10	0.04	0.13	**3.85**	**3.33**	0.17
Hypersaline	3.98	0.02	1.50	0.26	0.14	0.54	0.04	4.00	**1.90**	0.58
Inorganic	3.30	0.70	1.91	0.04	0.04	0.61	0.15	4.00	1.99	**0.76**
	3.53	0.47	1.75	0.10	0.15	0.57	0.00	4.00	2.00	0.57
	3.45	0.55	1.69	0.25	0.09	0.69	0.02	4.00	2.03	**0.71**
	3.37	0.63	1.74	0.18	0.14	0.65	0.00	4.00	2.06	0.65
	3.40	0.60	1.65	0.29	0.11	0.71	0.01	4.00	2.06	**0.72**
	3.28	0.72	1.93	0.08	0.06	0.59	0.00	4.00	2.07	0.59
	3.53	0.47	0.86	0.63	0.65	0.55	0.15	4.00	2.13	**0.70**
	3.81	0.19	0.01	2.83	0.05	0.12	0.21	4.00	2.90	0.33
	3.62	0.25	0.00	3.20	0.08	0.12	0.03	**3.87**	**3.28**	0.15

855 Estimated analytical errors are ±5% (σ) of the value for Na and K and ±3% (σ) for the other cations.

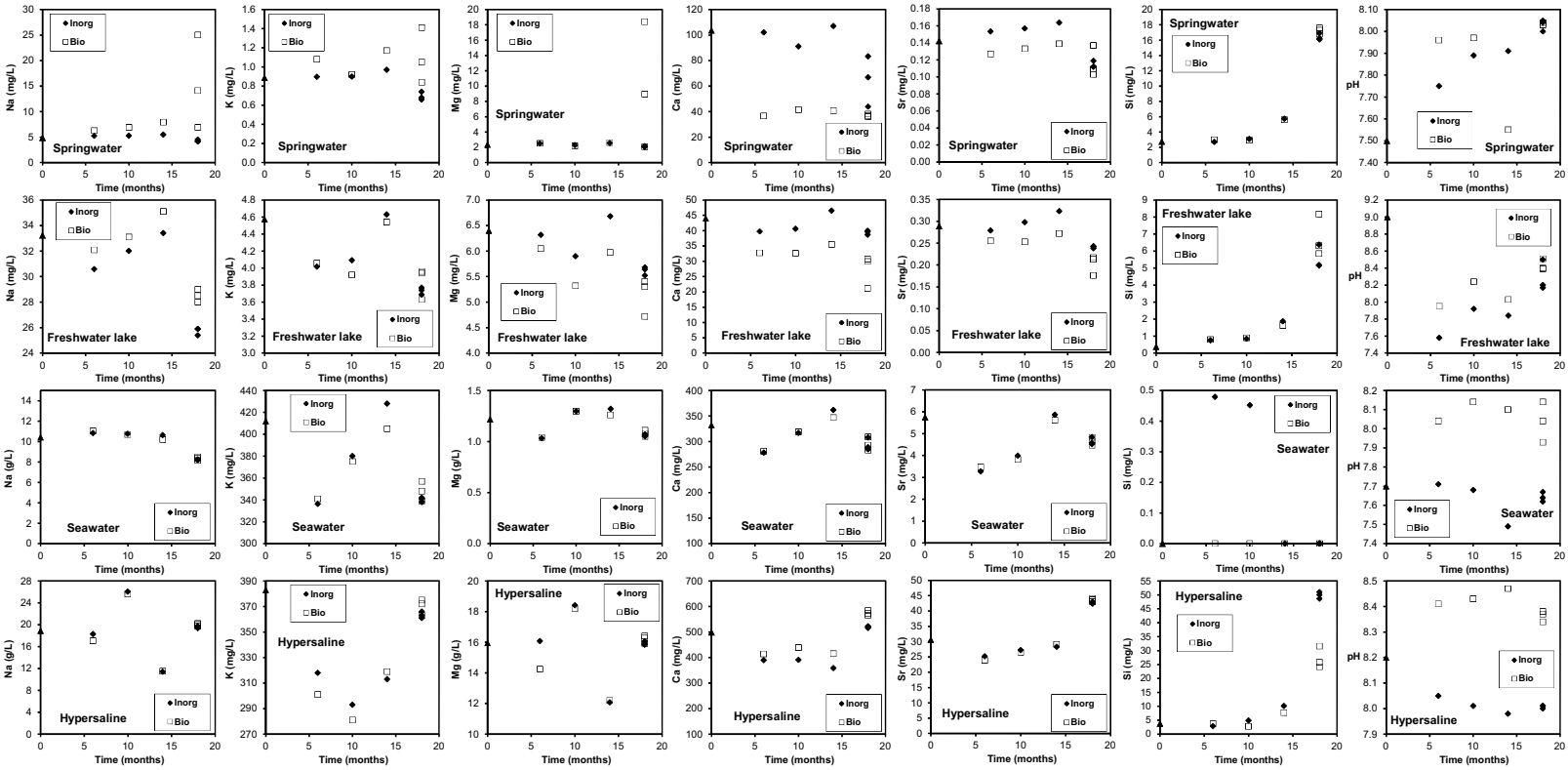
Na (mg/L)
K (mg/L)
Mg (mg/L)
Ca (mg/L)
Sr (mg/L)
Si (mg/L)
pH
Na (g/L)
K (g/L)
Mg (g/L)
Time (months)
Inorg
Bio
Springwater
Freshwater lake
Seawater
Hypersaline

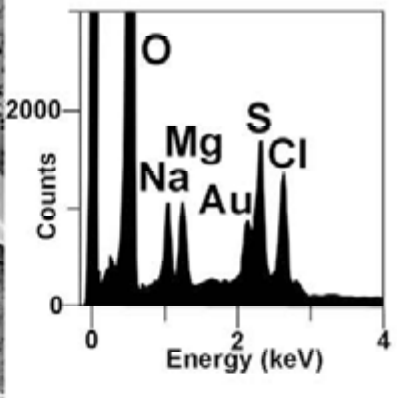

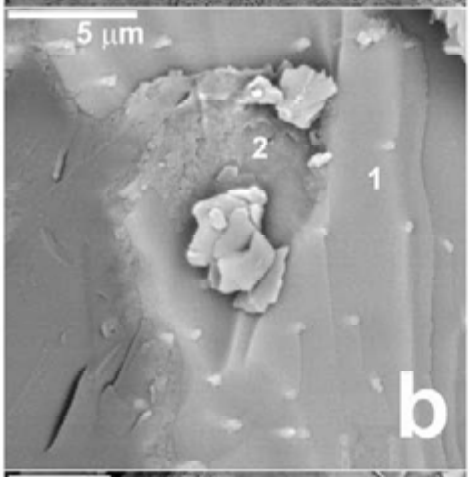

	Si	Al	Mg	Fe	K	Na
1)	100	20	0	na	3	4
2)	100	12	8	na	2	5

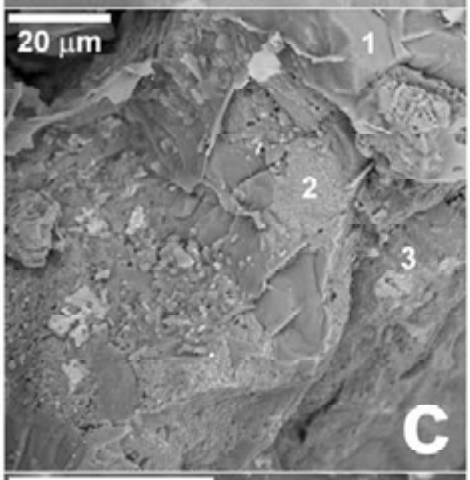

	Si	Al	Mg	Fe	K	Na
1)	100	13	2	3	2	2
2)	100	4	17	11	0	1
3)	100	12	8	14	0	3

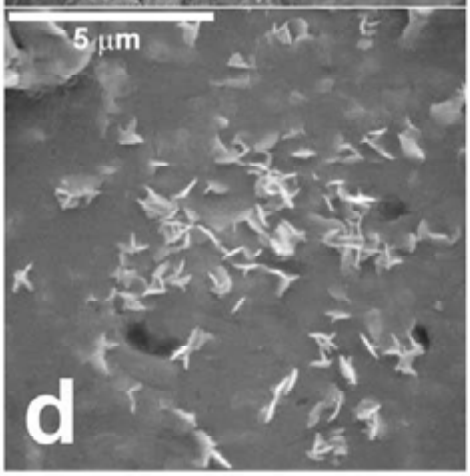

Fig 2

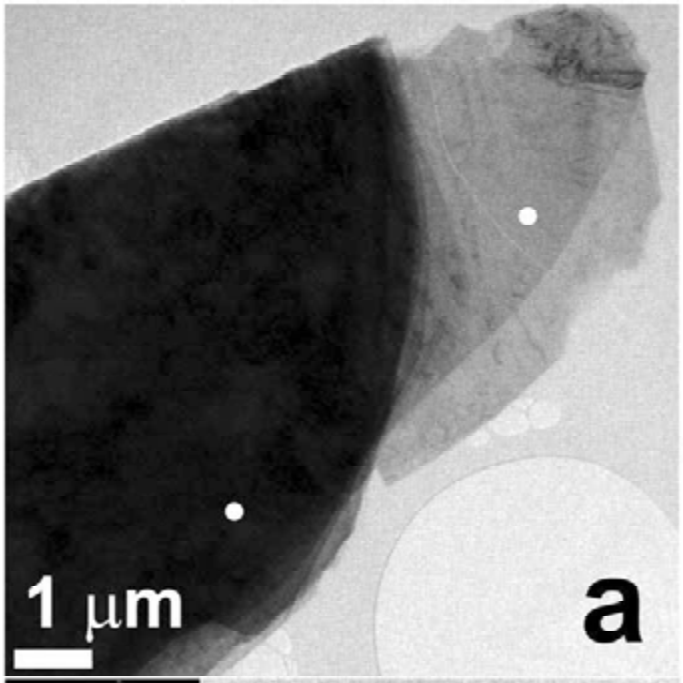
1 μm
a

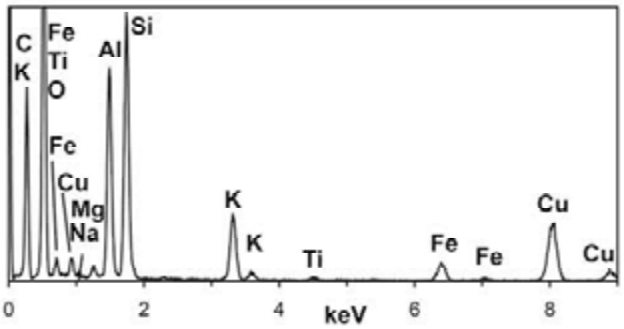
C K
Fe
Ti
O
Fe
Cu
Mg
Na
Al
Si
K
K
Ti
Fe
Fe
Cu
Cu
0
2
4
keV
6
8

Fig 3

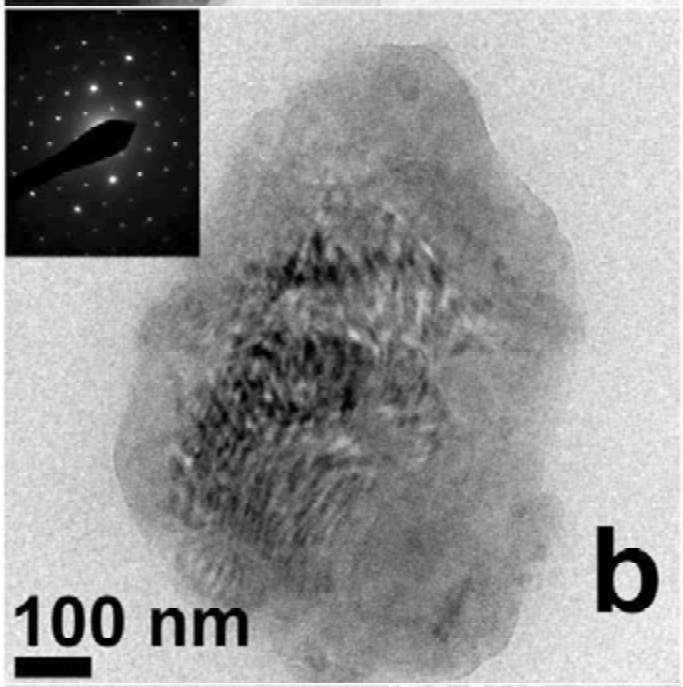
100 nm
b

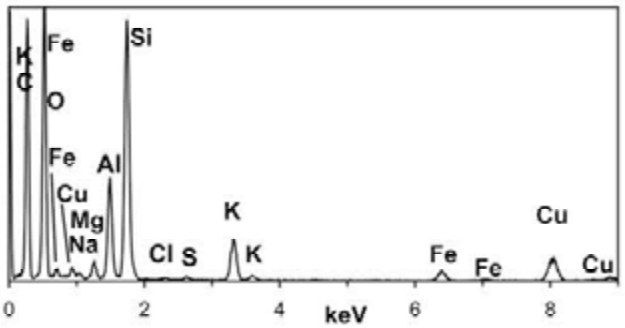
K C
Fe
O
Fe
Cu
Mg
Na
Al
Si
Cl
S
K
K
Fe
Fe
Cu
Cu
0
2
4
keV
6
8

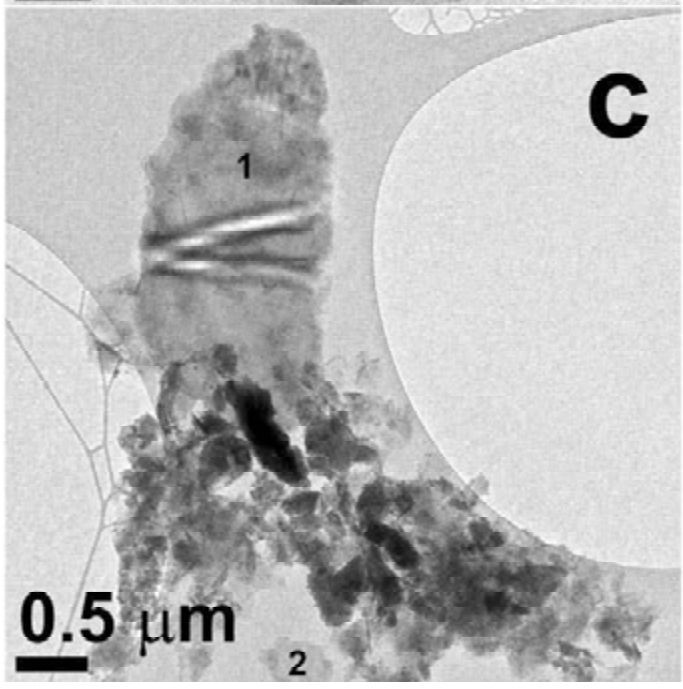
c
1
0.5 μm
2

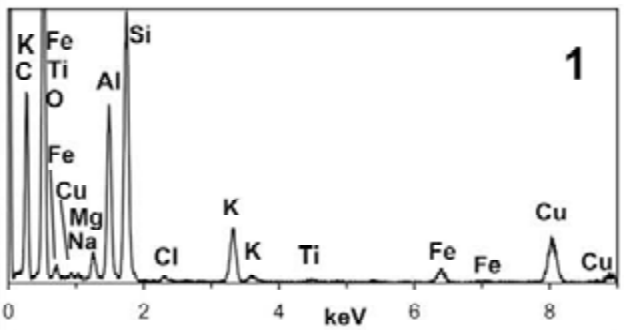
K C
Fe
Ti
O
Fe
Cu
Mg
Na
Al
Si
1
Cl
K
K
Ti
Fe
Fe
Cu
Cu
0
2
4
keV
6
8

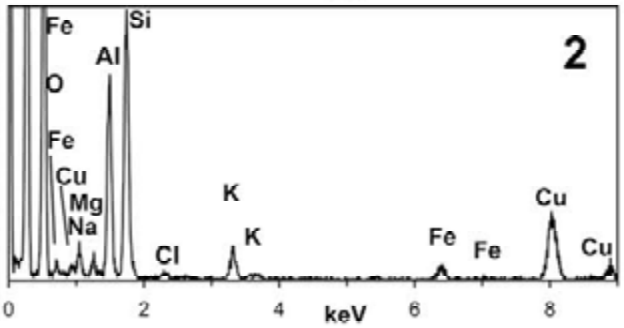
Fe
O
Fe
Cu
Mg
Na
Al
Si
2
Cl
K
K
Fe
Fe
Cu
Cu
0
2
4
keV
6
8

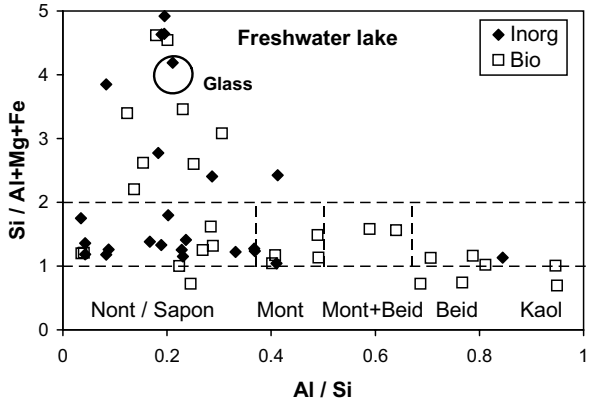
Freshwater lake
Inorg
Bio
Glass
Si / Al+Mg+Fe
Al / Si
Nont / Sapon
Mont
Mont+Beid
Beid
Kaol

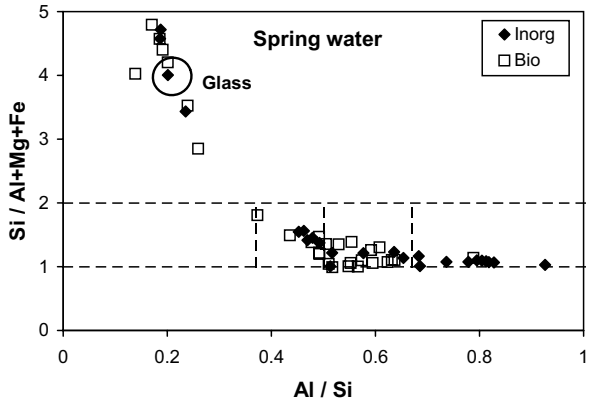
Spring water
Inorg
Bio
Glass
Si / Al+Mg+Fe
Al / Si

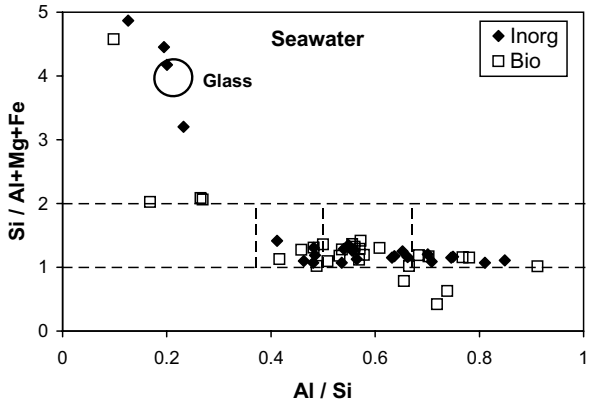
Seawater
Inorg
Bio
Glass
Si / Al+Mg+Fe
Al / Si

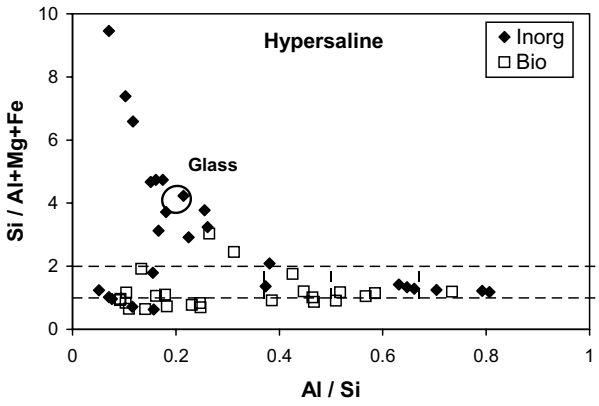
Hypersaline
Inorg
Bio
Glass
Si / Al+Mg+Fe
Al / Si

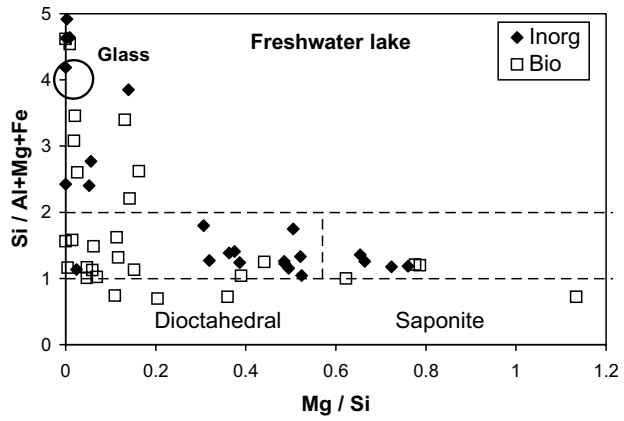
Freshwater lake
Inorg
Bio
Glass
Dioctahedral
Saponite
Si / Al+Mg+Fe
Mg / Si
0
1
2
3
4
5
0
0.2
0.4
0.6
0.8
1
1.2

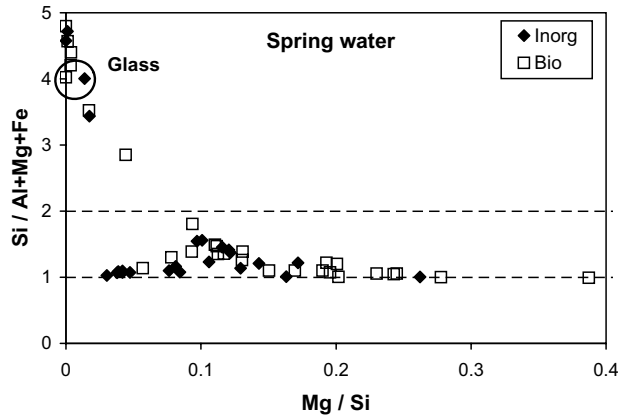
Spring water
Inorg
Bio
Glass
Si / Al+Mg+Fe
Mg / Si
0
1
2
3
4
5
0
0.1
0.2
0.3
0.4

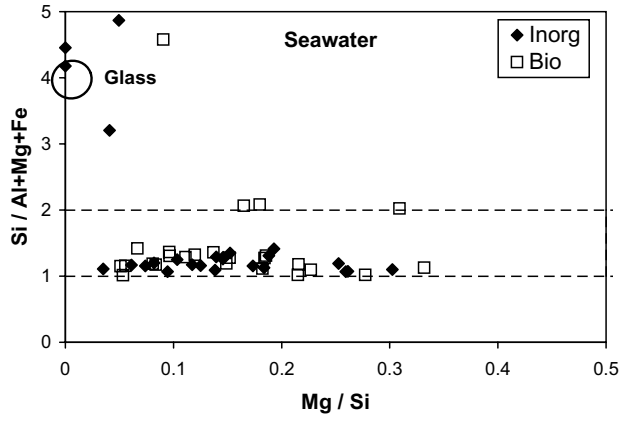
Seawater
Inorg
Bio
Glass
Si / Al+Mg+Fe
Mg / Si
0
1
2
3
4
5
0
0.1
0.2
0.3
0.4
0.5

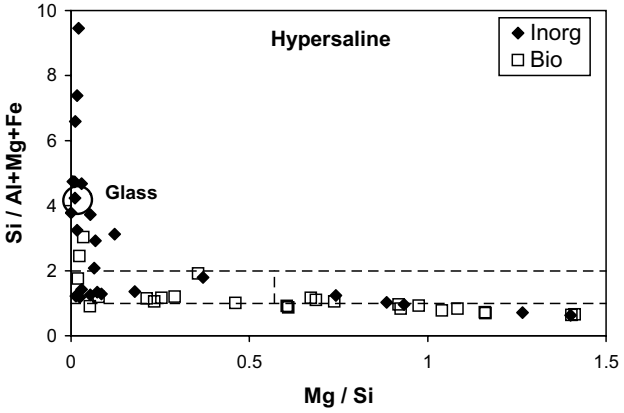
Hypersaline
Inorg
Bio
Glass
Si / Al+Mg+Fe
Mg / Si
0
2
4
6
8
10
0
0.5
1
1.5

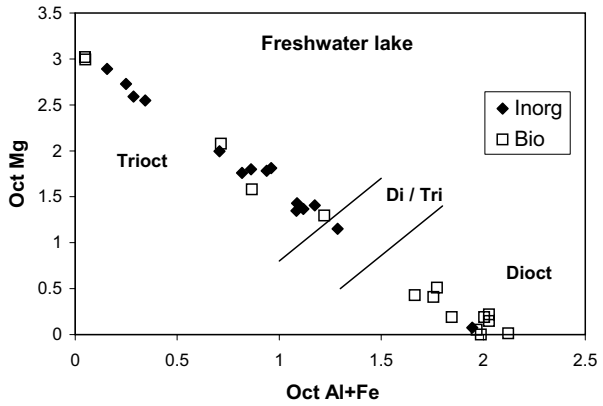
Freshwater lake
Inorg
Bio
Trioct
Di / Tri
Dioct
Oct Mg
Oct Al+Fe
0
0.5
1
1.5
2
2.5
3
3.5

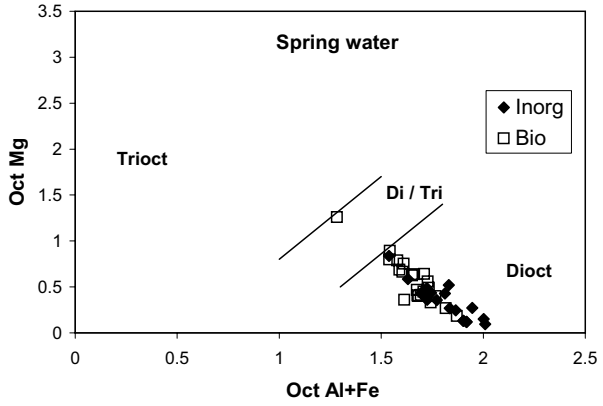
Spring water
Inorg
Bio
Trioct
Di / Tri
Dioct
Oct Mg
Oct Al+Fe
0
0.5
1
1.5
2
2.5
3
3.5

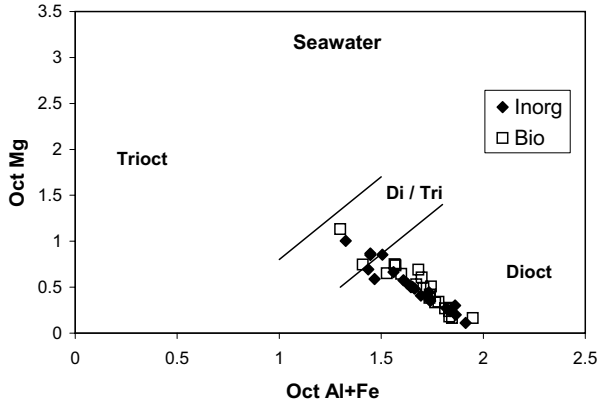
Seawater
Inorg
Bio
Trioct
Di / Tri
Dioct
Oct Mg
Oct Al+Fe
0
0.5
1
1.5
2
2.5
3
3.5

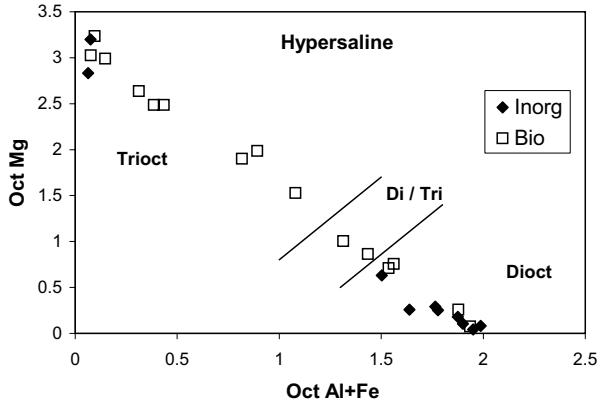
Hypersaline
Inorg
Bio
Trioct
Di / Tri
Dioct
Oct Mg
Oct Al+Fe
0
0.5
1
1.5
2
2.5
3
3.5

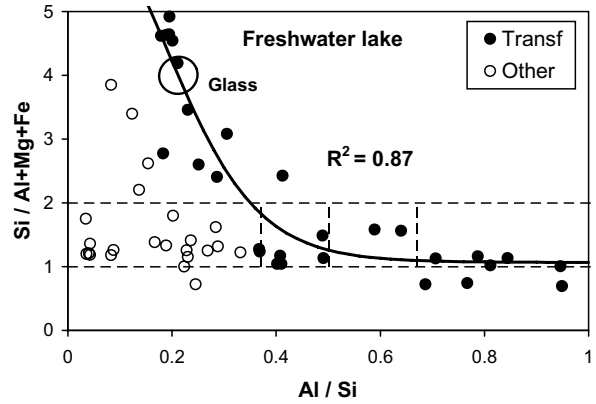
Freshwater lake
Transf
Other
Glass
R^2 = 0.87
Si / Al+Mg+Fe
Al / Si
0
1
2
3
4
5
0.2
0.4
0.6
0.8

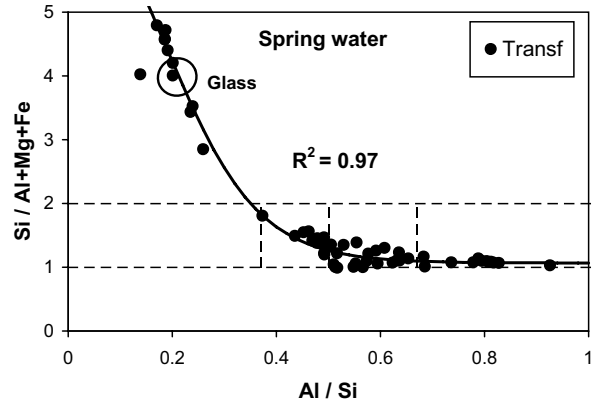
Spring water
Transf
Glass
R^2 = 0.97
Si / Al+Mg+Fe
Al / Si
0
1
2
3
4
5
0.2
0.4
0.6
0.8

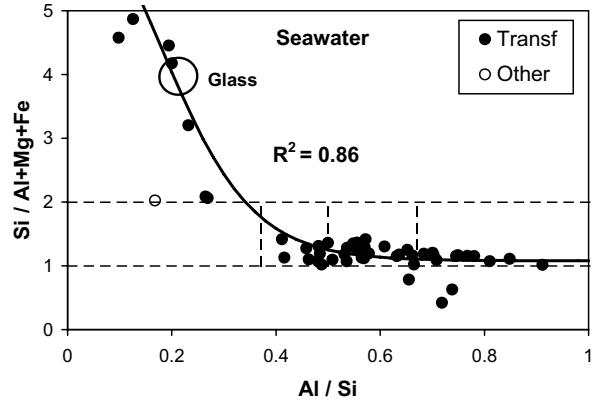
Seawater
Transf
Other
Glass
R^2 = 0.86
Si / Al+Mg+Fe
Al / Si
0
1
2
3
4
5
0.2
0.4
0.6
0.8

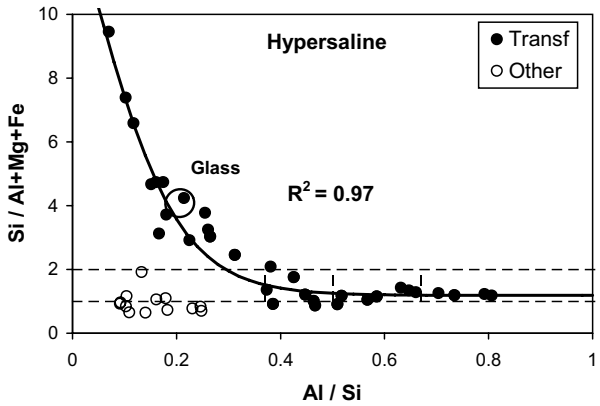
Hypersaline
Transf
Other
Glass
R^2 = 0.97
Si / Al+Mg+Fe
Al / Si
0
2
4
6
8
10
0.2
0.4
0.6
0.8

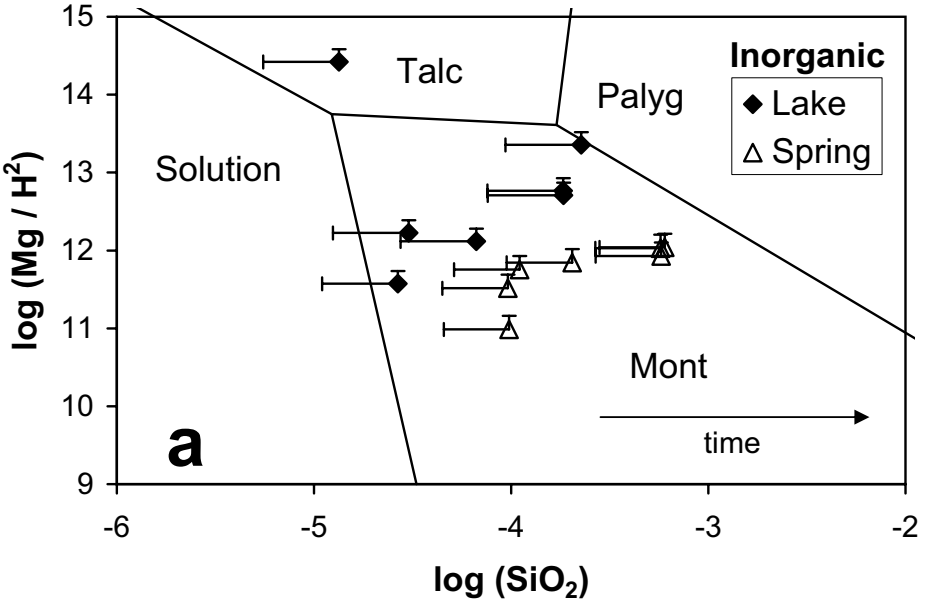
Talc
Palyg
Inorganic
Lake
Spring
Solution
Mont
time
a
log (Mg / H2)
log (SiO2)
15
14
13
12
11
10
9
-6
-5
-4
-3
-2

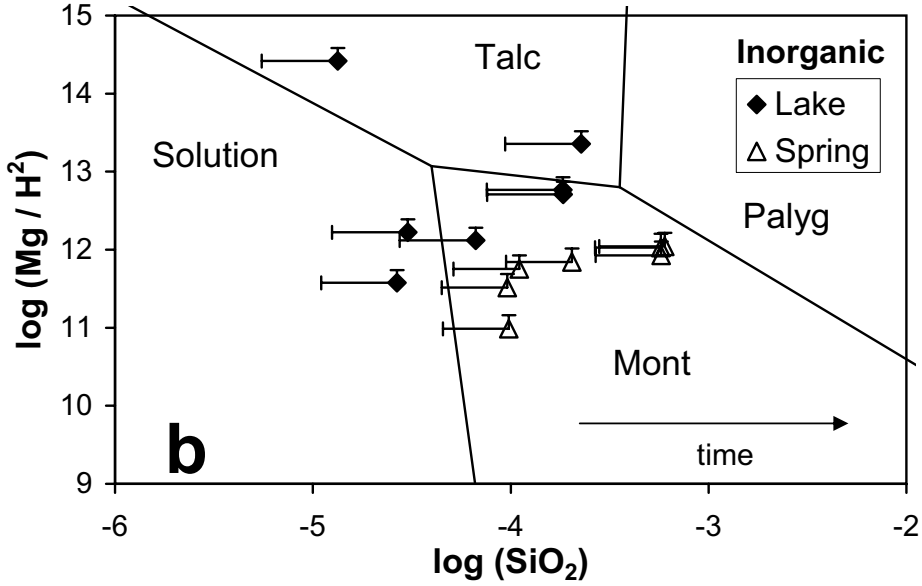
Talc
Inorganic
Lake
Spring
Solution
Palyg
Mont
time
b
log (Mg / H2)
log (SiO2)
15
14
13
12
11
10
9
-6
-5
-4
-3
-2